Metabolism 157 (2024) 155932

Contents lists available at ScienceDirect

Metabolism

journal homepage: www.journals.elsevier.com/metabolism

The evolutionary conserved miR-137/325 tandem mediates obesity-induced hypogonadism and metabolic comorbidities by repressing hypothalamic kisspeptin

María S. Avendaño [a,b,c,*,1], Cecilia Perdices-Lopez [a,b,c,1], Yolanda Guerrero-Ruiz [a,b], Francisco Ruiz-Pino [a,b], Ana B. Rodriguez-Sanchez [a,b,d], María J. Sanchez-Tapia [a,b], Verónica Sobrino [a,b], Rafael Pineda [a,b], Alexia Barroso [a,b], Alejandro Correa-Sáez [a,b], Maribel Lara-Chica [a,b], José C. Fernandez-Garcia [d,e], Ana B. García-Redondo [f,g,h], Raquel Hernanz [g,h,i], Miguel Ruiz-Cruz [a,b], David Garcia-Galiano [a,b], Nelly Pitteloud [j], Marco A. Calzado [a,b,c], Ana M. Briones [f,g,h], María J. Vázquez [a,b,c], Manuel Tena-Sempere [a,b,c,d,*]

[a] *Instituto Maimónides de Investigación Biomédica de Córdoba (IMIBIC), Córdoba, Spain*
[b] *Department of Cell Biology, Physiology and Immunology, University of Córdoba, Cordoba, Spain*
[c] *Hospital Universitario Reina Sofía, Córdoba, Spain*
[d] *CIBER Fisiopatología de la Obesidad y Nutrición (CIBEROBN), Instituto de Salud Carlos III, Córdoba, Spain*
[e] *Department of Endocrinology and Nutrition, Regional University Hospital of Málaga, Instituto de Investigación Biomédica de Málaga (IBIMA), Málaga, Spain*
[f] *Department of Pharmacology, Universidad Autónoma de Madrid, Madrid, Spain*
[g] *Instituto Investigación Hospital Universitario La Paz (IdiPaz), Madrid, Spain*
[h] *CIBER Enfermedades Cardiovasculares (CIBERCV), Instituto de Salud Carlos III, Madrid, Spain*
[i] *Department of Basic Health Sciences, Universidad Rey Juan Carlos, Madrid, Spain*
[j] *Department of Service of Endocrinology, Diabetes, and Metabolism, Faculty of Biology and Medicine, University of Lausanne, Lausanne University Hospital, Lausanne, Switzerland*

ARTICLE INFO

Keywords:
Obesity
Kiss1
Kisspeptins
MicroRNAs
miR-137
miR-325
Male hypogonadism
Comorbidities
Obesity-induced hypogonadism

ABSTRACT

Background: Obesity-induced hypogonadism (OIH) is a prevalent, but often neglected condition in men, which aggravates the metabolic complications of overweight. While hypothalamic suppression of *Kiss1*-encoded kisspeptin has been suggested to contribute to OIH, the molecular mechanisms for such repression in obesity, and the therapeutic implications thereof, remain unknown.

Methods: A combination of bioinformatic, expression and functional analyses was implemented, assessing the role of the evolutionary-conserved miRNAs, miR-137 and miR-325, in mediating obesity-induced suppression of hypothalamic kisspeptin, as putative mechanism of central hypogonadism and metabolic comorbidities. The implications of such miR-137/325-kisspeptin interplay for therapeutic intervention in obesity were also explored using preclinical OIH models.

Results: MiR-137/325 repressed human *KISS1* 3'-UTR in-vitro and inhibited hypothalamic kisspeptin content in male rats, while miR-137/325 expression was up-regulated, and *Kiss1*/kisspeptin decreased, in the medio-basal hypothalamus of obese rats. Selective over-expression of miR-137 in Kiss1 neurons reduced *Kiss1*/ kisspeptin and partially replicated reproductive and metabolic alterations of OIH in lean mice. Conversely, interference of the repressive actions of miR-137/325 selectively on *Kiss1* 3'-UTR in vivo, using target-site blockers (TSB), enhanced kisspeptin content and reversed central hypogonadism in obese rats, together with improvement of glucose intolerance, insulin resistance and cardiovascular and inflammatory markers, despite persistent exposure to obesogenic diet. Reversal of OIH by TSB miR-137/325 was more effective than chronic kisspeptin or testosterone treatments in obese rats.

* Corresponding authors at: Department of Cell Biology, Physiology & Immunology, Faculty of Medicine, University of Córdoba, Avda. Menéndez Pidal s/n., 14004 Córdoba, Spain.
E-mail addresses: b22avhem@uco.es (M.S. Avendaño), fi1tesem@uco.es (M. Tena-Sempere).
[1] These authors contributed equally to this work and should be considered as joint first authors.

https://doi.org/10.1016/j.metabol.2024.155932
Received 19 March 2024; Accepted 2 May 2024
Available online 8 May 2024

Conclusions: Our data disclose that the miR-137/325-Kisspeptin repressive interaction is a major player in the pathogenesis of obesity-induced hypogonadism and a putative druggable target for improved management of this condition and its metabolic comorbidities in men suffering obesity.
Significance statement: Up to half of the men suffering obesity display also central hypogonadism, an often neglected complication of overweight that can aggravate the clinical course of obesity and its complications. The mechanisms for such obesity-induced hypogonadism remain poorly defined. We show here that the evolutionary conserved miR137/miR325 tandem centrally mediates obesity-induced hypogonadism via repression of the reproductive-stimulatory signal, kisspeptin; this may represent an amenable druggable target for improved management of hypogonadism and other metabolic complications of obesity.

1. Introduction

Obesity is a complex multifactorial condition that has reached pandemic proportions, with nearly 60 % of the adult European population suffering overweight or obesity (https://apps.who.int/iris/bitstream/handle/10665/353747/9789289057738-eng.pdf), and an overall prevalence of obesity >41 % in US (https://www.cdc.gov/obesity/data/adult.html). Obesity is one of the main (if not the most relevant) preventable risk factor for multiple comorbidities, including cardiometabolic diseases and some types of cancer, causing increasing mortality rates and worsening the course of multiple pathologies, from diabetes and hypertension to COVID-19 [1–3]. Notably, obesity has been shown to be associated also to different forms of gonadal and reproductive dysfunction, including, prominently, central male hypogonadism, characterized by a decrease in circulating levels of luteinizing hormone (LH), as pituitary driver of testicular androgen production, and testosterone [4,5]. Yet, this condition remains largely over-looked and the actual prevalence of obesity-induced hypogonadism (OIH) in men, also termed male-obesity secondary hypogonadism, is controversial, although recent publications point out that up to half of obese men over 40 years of age have circulating levels of total testosterone below 10.4 nmol/L, namely biochemical hypogonadism, whose frequency increases with age [5–7].

The pathophysiological relevance of OIH clearly exceeds the reproductive dimension. In fact, the interplay between obesity and hypogonadism defines a sort of vicious circle, worsening each other, and their cardiometabolic comorbidities. In one hand, male hypogonadism is known to promote increased adiposity, adverse adipokine profiles and insulin resistance in men, via as yet partially unknown mechanisms. In turn, obesity favours the instauration and progression of hypogonadism, likely via multiple mechanisms, including enhanced aromatase activity in the adipose, increased inflammatory mediators and leptin levels, insulin resistance and, relevantly, deregulation of key central pathways controlling the reproductive axis. This reciprocal harmful interplay is reinforced by common comorbidities, e.g., diabetes, which worsen the prognosis of OIH and promote its self-perpetuation [8–11]. Hence, interruption of this vicious circle is deemed essential not only to prevent the reproductive deficits but, more importantly, also to improve the course and management of the whole set of metabolic disorders linked to obesity.

Although the mechanisms putatively involved in OIH remain ill defined, compelling, as yet fragmentary evidence has suggested the potential role of alterations of the hypothalamic Kiss1 system [12–14]. Kisspeptins, the product of *Kiss1* gene that operate via the G-protein coupled receptor, Gpr54 (aka, Kiss1r), have recently emerged as master elements of the central control of the gonadal axis, mainly by activating hypothalamic neurons producing gonadotropin-releasing hormone (GnRH) [15]. Inactivating mutations of the genes encoding kisspeptins or their receptor are bound to central hypogonadism in rodents and humans [16–18], while adverse conditions, ranging from subnutrition or diabetes to inflammation [19–21], that suppress the hypothalamic Kiss1 system, lead to inhibition of the gonadal axis in pre-clinical models. In the physiological setting, kisspeptins are mainly produced by discrete neuronal populations within the hypothalamus, located either in the arcuate nucleus (ARC; or its equivalent infundibular area in humans) or the rostral hypothalamus, particularly in the anteroventral periventricular (AVPV) region in rodents [15]. Of note, while the AVPV population of Kiss1 neurons is especially prominent in females and mainly involved in the control of ovulation, the ARC population of Kiss1 neurons is present in both sexes and has been shown to play a crucial role in the control of the tonic, pulsatile secretion of GnRH, and hence gonadotropins, responsible for the regulation of gonadal function [22]. ARC expression of *Kiss1* has been shown to be suppressed in models of diet-induced obesity in male rats and mice [12–14]. Yet, the mechanism (s) for such obesity-induced suppression remains unknown.

ARC Kiss1 neurons not only display a complex developmental program, but are also endowed with sophisticated regulatory systems, involving genetic but also epigenetic mechanisms [15,23]. On the latter, small non-coding RNAs, named microRNAs (miRNAs), have emerged as pivotal elements in epigenetic control of a myriad of functions, both in health and disease [24]. MiRNAs are small RNA sequences, about 22-nt long, which can bind, via specific seed regions, to discrete sequences mainly located at the 3′-untranslated region (3'-UTR) of target genes, and operate mainly as negative regulators of target mRNAs, either by preventing their translation or promoting their degradation [25]. Of note, one single miRNA can bind multiple gene targets, while one gene can be modulated by different miRNAs [26]. This multiplicity allows the generation of sophisticated regulatory networks that can modulate complex biological processes in an integral manner [27]. Recent evidence has suggested a major role of specific miRNAs in the control of GnRH neurons, as key mechanism for pubertal control [28], while we have very recently documented an essential function of canonical miRNA biogenesis in Kiss1 neurons for adult gonadal function [29]. On the other hand, hypothalamic miRNA expression is seemingly sensitive to metabolic conditions, including obesity [30], while as yet scarce evidence has suggested that human *KISS1* might be direct target of miRNA regulation in other tissues, as the placenta [31]. Yet, the eventual pathophysiological role of specific miRNA pathways in the direct control of hypothalamic *Kiss1* has not been explored to date. We report herein that the conserved miRNA tandem, miR-137/miR-325, operates as direct repressor of hypothalamic kisspeptin and, thereby, contributes to OIH and its metabolic comorbidities.

2. Materials and methods

2.1. Ethic statement

The experimental procedures were approved by the corresponding local (Córdoba University) and regional (Junta de Andalusia) Ethical Committees for Animal Experimentation and were conducted in accordance with the European Union normative for care and use of experimental animals.

2.2. Animals

Male Wistar rats were bred in the vivarium of the University of Córdoba at IMIBIC. The day the animals were born was considered day 1 of age. The animals were kept under constant conditions of light (12 h of

light, from 7:00 am) and temperature (22 °C). They were weaned on postnatal day (PND) 21 and were provided with free access to tap water and pelleted food (A04, Panlab; 2.90 Kcal/g), unless otherwise stated.

The mouse line, *Kiss1*$^{Cre:GFP}$ (v2) (RRID:IMSR_JAX:033169) was generated by Prof. Richard Palmiter (University of Washington, Seattle, WA), as reported elsewhere [32]. This *Kiss1*$^{Cre:GFP}$ model holds a Cre recombinase cassette, fused to GPF reporter coding sequence, in the first exon of the *Kiss1* allele, thereby allowing expression of Cre and GFP in *Kiss1*-expressing cells.

The mouse line *Kiss1*$^{Cre:EYFP}$ was generated by crossing the *Kiss1*$^{Cre:GFP}$ *(v2)* mouse with the R26R-EYFP mouse (B6.129X1-Gt(ROSA) 26Sortm1(EYFP)Cos/J; RRID:IMSR_JAX:006148) [33]. In *Kiss1*$^{Cre:EYFP}$ mice, Cre recombinase activity, driven by the Kiss1 promoter, deletes the stop sequence coupled to EYFP locus and allows strong expression of the fluorescent marker in Kiss1 cells of the double mutant mice.

2.3. Generation of the OIH rat model

A rat model of early-onset obesity associated to hypogonadism, previously validated in our group [13], was used. On postnatal day-1 (PND1), newborn male rats were randomly grouped following a cross-fostering protocol. Pups were assigned to two different litter sizes: normal litter (NL, 12 pups male per litter) or small litter (SL, 4 pups male per litter). After weaning on PND21, the NL group was fed with low fat diet (LFD; referred also as control diet: CD), D12450B (10 % of calories from fat, 20 % from protein, and 70 % from carbohydrate), while the SL group was fed with high fat diet (HFD), D12451 (45 % of calories from fat, 20 % from protein, and 35 % from carbohydrate; Research Diets Inc).

2.4. Drugs

Rat kisspeptin-10 (Kp-10; KISS-1 (110–119)-NH_2), analogue of the human C-terminal KISS-1 decapeptide KISS-1 (112−121)-NH_2, was obtained from Phoenix Pharmaceuticals. A dose of 10 pmol, as capable to sub-maximally elicit LH and FSH secretion was employed [34]. Kp-10 was dissolved in physiological saline (0.9 % sodium chloride) and administered intracerebroventricularly (icv) in a final volume of 5 μL. Glucose (GL01271000, Scharlab, Spain) and insulin (mouse: ref. 2643, rat: ref. 109,081; Sigma Chemical Co., USA) were administered intraperitoneally (ip). Testosterone (T, 17β-Hydroxy-3-oxo-4-androstene; Sigma-Aldrich, St Louis, MO, USA) was subcutaneously implanted with silastic capsules [length 2 cm; inner diameter (ID) 1.98 mm; outer diameter (OD) 3.18 mm; Dow Corning, Seneffe, Belgium]. For glucose tolerance tests (GTT), a bolus of 1 g/kg of BW per rat was employed. For insulin tolerance tests (ITT), one international unit (IU) bolus/kg BW was (ip) administered. Acetylcholine (ACh) and phenylephrine (Phe) were purchased from Sigma-Aldrich.

2.5. Experimental designs

In ***Experiment 1***, we performed in vitro validation of predicted repressive action of miR-137-3p and miR-325-3p on 3' UTR of *KISS1* by performing the Secrete-Pair dual luciferase assay in HEK293 cells (human embryonic kidney cells). *KISS1* 3'UTR Gaussia luciferase (Gluc) reporter construct (217HmiR010098-MT05), precursor expression plasmids for hsa-miR-137-3p (217HmiR0011-MR04-B) and hsa-miR-325-3p (217MmiR33334-MR04), and precursor miRNA scrambled control plasmid (217CmiR0001-MR04) were obtained from GeneCopeia (Rockville, MD, USA). Transient transfections were performed with Rotifect (Carl Roth, Karlsruhe, Germany) according to manufacturer's instructions (Promega, Madison, WI, USA). In detail, Secrete Pair Dual Luminescence Assay was performed following the manufacturer's instruction. HEK293 cells were maintained in DMEM (Dulbecco's modified Eagle's medium; Life Technologies, Grand Island, NY, USA) supplemented with 10 % FBS (fetal bovine serum), 2 mM L-glutamine and 1 % (*v*/v) penicillin/streptomycin at 37 °C in a humidified atmosphere containing 5 % CO_2. Cells were co-transfected with (i) *KISS1* 3'-UTR Gluc reporter construct, (ii) *KISS1* 3'-UTR Gluc and scrambled miRNA vectors, (iii) 3'-UTR control construct and hsa-miR-137-3p or hsa-miR-325-3p expression vectors, and (iv) *KISS1* 3'UTR Gluc construct and hsa-miR-137-3p or hsa-miR-325-3p expression vectors, at a concentration ratio 1:4 (250 ng:1000 ng), respectively. Transfections were performed using three to five replicates for each experimental condition. Cells were collected in PBS after 24 h and lysated following the instructions of the luciferase assay kit. Luciferase activity was measured using an Autolumat LB 9510 (EG&G Berthold, USA).

In ***Experiment 2***, the hypothalamic expression of miR-137-3p and miR-325-3p was analyzed in our OIH male rat model. To this end, hypothalamic samples encompassing the mediobasal hypothalamus (MBH) or the preoptic area (POA), were obtained, as described in the following section. The expression levels of *Kiss1* mRNA, miR-137-3p and miR-325-3p, as well as kisspeptin protein content, were measured as described in detail in following sections.

In ***Experiment 3***, the central regulatory role of miR-137-3p on reproductive function was evaluated using a miRCURY LNA miRNA mimic, designed to simulate the natural miR-137-3p miRNA, which was administered centrally to adult young male rats, bred at NL and fed ad libitum (control conditions). Mimic miR-137-3p was injected icv (0.2 mm posterior to bregma line; 1.2 mm lateral to bregma and 3 mm depth) daily, from PND60 to PND75. Mimic miR-137-3p (MiRCURY LNA miRNA mimics, Qiagen) was mixed with in vivo-jetPEI® (Polyplus®) in a jetPEI/nucleic acid ratio of 7, following manufacturer instructions. A dose of 40 pmol/5 μL was administered daily during the period of treatment. Rats treated with vehicle (5 % glucose-JetPEI) served as controls (n = 10–12 per group). At the end of the experiment, we collected blood samples, to analyze circulating levels of LH and testosterone, and hypothalamic tissue. Hypothalamic samples were analyzed by western blot to validate the effect of the miRNA mimic on kisspeptin content.

In ***Experiment 4***, we assessed the functional role of miR-137-3p specifically in *Kiss1*-expressing neurons. To this end, we performed stereotaxic injections in the ARC of the hypothalamus of an adeno-associated viral vector expressing miR-137-3p in the mouse lines, *Kiss1*$^{Cre:GFP}$ *(v2)* and *Kiss1*$^{Cre:EYFP}$. The viral vector, VB210304–1205 XHC (Vector Builder, Chicago), was designed to contain an inverted sequence of mmu-miR-137 and mCherry reporter, flanked by loxP sites with opposite direction. The inversion of the flanked sequenced is prompted by the Cre recombinase that is active specifically in Kiss1-expressing cells in the above mouse models. In detail, adult *Kiss1*$^{Cre:GFP}$ male mice (PND90) were bilaterally injected with 200 nL of the viral vector, titrated to 5 × 10^{12} genome copies (gc)/mL by dilution in TE buffer 1× (− 2.1 mm posterior to bregma, 0.25 mm to each lateral of the midsagittal suture and −5.9 mm, dorsoventrally). Control mice were infected with scramble viral vector containing mCherry solely, flanked by LoxP sites. Expression of the virus was allowed until PND150, when mice were euthanized. Body weight and food intake were followed weekly, body composition was analyzed before and at the end of the experiment (n = 3/11 per group). At that time, blood was collected and mice were perfused to fix the brain to perform immunohistochemistry analysis (n = 3 per group). In parallel, adult *Kiss1*$^{Cre:EYFP}$ male mice (PND90) were unilaterally injected with 200 nL (2.38 × 10^{13} gc/mL) of the viral vector using the same coordinates as above and were maintained during one month (n = 4 per group). After that time, mice were euthanized, mediobasal hypothalamus were extracted and FACS sorting was performed to isolate EYFP+ expressing neurons and EYPF+/mCherry + neurons.

In ***Experiment 5***, the effects of preventing the repressive action of miR-137/miR-325 on *Kiss1* 3'-UTR were assessed in our model of OIH. Male rats were randomly reared in NL or SL, from PND1. After weaning at PND21, NL rats were fed ad libitum with control diet, while SL rats received HFD. At PND150, SL/HFD rats (n = 24) were allocated to two

experimental groups and treated from PND150 to PND166, as follows: (1) SL/HFD control group ($n = 12$), treated with vehicle (VEH, TE 1× buffer); (2) SL/HFD TSB miR-137/325 group (n = 12), treated icv with Target site blockers (TSB) against miR-137/325 (100 pmol/5 μL) once every 4 days. TSB are selective and specific RNA sequences, custom-designed with phosphor-thioate backbone modifications, from Qiagen (miRCURY LNATM microRNA Target Site Blockers, in vivo ready). TSB miR-137/325 sequence (5'-TTATTGCACAAGTCTA-3′) prevents binding of miR-137-3p/ miR-325-3p specifically to the 3' UTR of *Kiss1*, therefore blocking the repressive actions of these miRNAs. A group of NL/CD rats ($n = 12$) treated with vehicle served as control.

Analyses in these experimental groups included pre-treatment body composition, follow-up of body weight and food intake, GTT and ITT. During treatment, periodic blood extraction was performed an hour after treatment injection. At the end of the treatment, systolic blood pressure, body composition, GTT and ITT were assessed. Upon euthanasia, hypothalamic tissue was collected for expression analyses, while different parameters cardiovascular performance were analyzed, as described in the next sections.

In ***Experiment 6,*** a similar model of OIH and their corresponding controls were used to assess the effects of testosterone (T) replacement or repeated Kp-10 injections on different reproductive, hormonal and metabolic indices. To this end, at PND150, SL/HFD rats ($n = 36$) were allocated to three experimental groups and treated from PND166 to PND180, as follows: (1) SL/HFD control group ($n = 12$), treated with vehicle (saline); (2) SL/ HFD Kp-10 group (n = 12), treated twice daily icv with 10 pmol/5 μL of kisspeptin-10, and (3) SL/HFD Testosterone group (n = 12), subcutaneously implanted with silastic capsules containing testosterone. Phenotypic analysis included pre-treatment body composition, follow-up of body weight and food intake, as well as GTT, ITT and systolic blood pressure measurements. During treatment, blood extraction was performed one hour after Kp-10 injection (or equivalent time in T-treated groups), on days 1, 4 and 8 of treatment. Blood samples and hypothalamic tissue were collected at the end of the experiment.

2.6. General analytical procedures

Body weight (BW) gain and daily energy intake. BW gain, terminal BW, and daily energy intake were monitored. Daily energy intake was calculated using the kilocalories per gram information provided by the diet manufacturer (3.85 kcal/g for LFD; 4.73 kcal/g for HFD), after assessing daily food consumption.

Body composition by quantitative magnetic resonance (QMR) analysis. Percentage of lean and fat mass (body composition) was analyzed in experimental animals by quantitative magnetic resonance (QMR), using the EchoMRI™ 700 analyzer (Houston, TX, software v.2.0). Adiposity index was calculated as follows: [fat mass (%) / fat + lean mass (%)] x100.

Glucose tolerance tests (GTT). At the end of the treatments, the different experimental groups were weighed and fasted overnight. Basal glucose levels were recorded at 8:00 to 9:00 AM. A bolus of glucose (1 g/kg BW) was applied by intraperitoneal injection, and glucose concentrations were measured at 20, 60 and 120 min.

Insulin tolerance tests (ITT). At the end of the treatments, the different experimental groups were weighed and fasted overnight. Basal glucose levels were recorded at 8:00 to 9:00 AM. A bolus of insulin (1 UI/kg BW) was applied by intraperitoneal injection, and glucose concentrations were measured at 20, 60, and 120 min.

Systolic blood pressure (SBP). SBP was measured in conscious rats by tail-cuff plethysmography (CIBERTEC Niprem 2000, Non-Invasive Blood Pressure System), before and after treatments, in warm conditions with an overhead heating lamp, to better detect the pulse of the animals. Prior to register SBP data (Niprem 1.5 software), animals were habituated to the experimental protocol. For each animal, several blood pressure readings were obtained and averaged, being expressed as mmHg.

Cardiac hypertrophy determination. Hearts were removed and the length of the tibia was annotated. The ratio between dry weight of heart and the length of the tibia was calculated.

Relative prostate weight. Prostates were dissected and removed for assessing prostate hypertrophy, evaluated as 'prostate dry weight (mg) / body weight (BW) (g) x 100'.

Sample collection. For hypothalamic collection, brains were placed on foil paper over dry ice, with the hypothalamus upwards until they got frozen, and were stored at −80 °C. For mRNA, miRNA and western blot (WB) procedures, the hypothalami were placed on ice, mild-thaw and dissected from the brain. To analyze independently POA and MBH, POA was dissected from MBH by a coronal cut posterior to the optic chiasm. For immunohistochemistry analyses, mice were intraperitoneally anesthetized with ketamine/ xylazine in a 2:1 proportion. Next, mice were perfused with 0.9 % saline followed by 4 % of para-formaldehyde (PFA). Whole brains were collected, postfixed in PFA during 24 h at 4 °C, washed in phosphate buffer saline (PBS) for 24 additional hours and dehydrated in sucrose at 30 % in PBS 0.1 M for 48 h. Blood, for hormonal and cytokine measurement, was obtained by jugular venipuncture or trunk collection after decapitation of the animals. Serum was stored at −20 °C after centrifugation at 3000*g* for 20 min.

2.7. Vascular analyses

Vascular tissue preparation. Third order branches of the mesenteric artery were removed and placed in cold (4 °C) Krebs-Henseleit solution (KHS) (115 mM NaCl, 25 mM $NaHCO_3$, 4.7 mM KCl, 1.2 mM $MgSO_4.7H_2O$, 2.5 mM $CaCl_2$, 1.2 mM KH_2PO_4, 11.1 mM glucose, and 0.01 mM Na_2EDTA) bubbled with a 95 % O_2–5% CO_2 mixture (pH = 7.4). Studies of vascular structure and function were made on the same day on fresh tissue.

Vascular function. Reactivity of rat mesenteric artery was studied in a wire myograph, according to previous references [35]. After a 30-min equilibration period in oxygenated KHS, arterial segments were stretched to their optimal lumen diameter for active tension development. Contractility of segments was then tested by an initial exposure to a high-K^+ solution (K^+-KHS, 120 mM). The presence of endothelium was determined by the ability of 10 μM ACh to relax arteries precontracted with Phe at approximately 50 % of K^+-KHS contraction. Afterwards, a single concentration-response curve to ACh (1 nM-10 μM) and Phe (0.1 μM–30 μM) was performed. All drugs were initially dissolved in distilled water; further dilutions were made in distilled water.

Pressure myography. The structural and mechanical properties of mesenteric resistance arteries were studied with a pressure myograph (Danish Myo Tech, Model P100, J.P. Trading I/S, Aarhus, Denmark), according to previously published protocols [36]. Vessels were placed on two glass microcannulae and secured with surgical nylon suture. After any small branches were tied off, vessel length was adjusted so that the vessel walls were parallel without stretch. Intraluminal pressure was then raised to 140 mmHg and the artery was unbuckled by adjusting the cannulae. The segment was then set to a pressure of 70 mmHg and allowed to equilibrate for 60 min at 37 °C in calcium-free KHS ($0Ca^{2+}$; omitting calcium and adding 1 mM EGTA) intravascular and extravascular perfused, gassed with a mixture of 95 % O_2 and 5 % CO_2. Intraluminal pressure was reduced to 3 mmHg. A pressure-diameter curve was obtained by increasing intraluminal pressure in 20 mmHg steps from 3 to 140 mmHg. Internal and external diameters were continuously measured under passive conditions (D_{i0Ca}, D_{e0Ca}) for 3 min at each intraluminal pressure. The final value used was the mean of measurements taken during the last 30 s, when the measurements reached steady state.

Calculation of passive structural and mechanical parameters. From internal and external diameter measurements in passive conditions, the following structural and mechanical parameters were calculated with the formulas:

$$\text{Wall thickness (WT)} = (D_{e0Ca} - D_{i0Ca})/2; \text{Wall : lumen} = (D_{e0Ca} - D_{i0Ca})/2D_{i0Ca}$$

Incremental distensibility represents the percentage of change in the arterial internal diameter for each mmHg change in intraluminal pressure and was calculated according to the formula:

$$\text{Incremental distensibility} = \Delta D_{i0Ca}/(D_{i0Ca} \times \Delta P) \times 100$$

Circumferential wall strain (ε) = (D_{i0Ca} - D_{00Ca})/D_{00Ca}, where D_{00Ca} is the internal diameter at 3 mmHg and D_{i0Ca} is the observed internal diameter for a given intravascular pressure both measured in 0Ca^{2+} medium.

Circumferential wall stress (σ) = (P × D_{i0Ca})/(2WT), where P is the intraluminal pressure (1 mmHg = 1.334 × 10^3 dynes·cm^{-2}) and WT is wall thickness at each intraluminal pressure in 0Ca^{2+}-KHS.

Arterial stiffness independent of geometry was determined by Young's elastic modulus (E = stress/ strain).

The stress-strain relationship is non-linear; consequently, it is more appropriate to obtain a tangential or incremental elastic modulus (E_{inc}) by determining the slope of the stress-strain curve ($E_{inc} = \delta\sigma/\delta\varepsilon$). E_{inc} was obtained by fitting the stress-strain data from each animal to an exponential curve using the equation: $\sigma = \sigma_{orig}e^{\beta\varepsilon}$, where σ_{orig} is the stress at the original diameter (diameter at 3 mmHg). Taking derivatives on the equation presented earlier, we see that $E_{inc} = \beta\sigma$. For a given σ-value, E_{inc} is directly proportional to β. An increase in this β index implies an increase in E_{inc}, which means an increase in stiffness.

2.8. Hormonal and metabolic analyses

Serum LH and FSH levels were measured using RIA kits supplied by the National Institutes of Health (Dr. A.F. Parlow, National Hormone and Peptide Program, Torrance, CA, USA). Hormonal determinations were performed in duplicates. Rat LH-I-10 and FSH-I-9 were labelled with ^{125}I by the chloramine-T method, and hormone concentrations were expressed using reference preparations LHRP-3 and FSH-RP-2 as standards. Intra- and inter-assay coefficients of variation were <8 % and 10 % for LH and 6 % and 9 % for FSH, respectively. The sensitivity of the assay was 5 pg/tube for LH and 20 pg/tube for FSH. Accuracy of hormone determinations was confirmed by assessment of rat serum samples of known concentrations (external controls). Testosterone levels from serum samples were determined using the ImmunoChem™ Testosterone Double Antibody RIA Kit (MP07189102, MP Biomedical™, USA). Intra and inter assay coefficients of variation were 10 % and 11 %, respectively. The sensitivity of the assay was 0.1 ng/mL. Leptin levels were measured with Multi-Species Leptin RIA kit (XL-85 K, Merck). Sensitivity was 0.801 ng/mL +2SD, and coefficients of intra-assay and inter-assay variation were 3.22 % and 7,75 %, respectively. Insulin levels were measured with Rat Insulin RIA kit (RI-13 K, Merck). Sensitivity was 0.081 ng/mL + 2SD and coefficients of intra-assay and inter-assay variation were 2.86 % and 9 %, respectively. Glucose levels were assayed using a glucometer (ACCU-CHEK) from Aviva (Roche Diagnostics).

2.9. Protein analysis by western blot

Protein samples were obtained by precipitation with acetate of the flow through obtained with mRNA Purification kit (Favorgen). Protein concentration was determined using RC DC™ Protein Assay (Bio-Rad), to equalize concentration levels between samples. Before western blots, absorbance of the samples was quantified by spectrophotometry (Beckman DU530). Twenty μg of protein per sample were submitted to SDS-PAGE on 7 % polyacrylamide gels, electro-transferred on polyvinylidene difluoride (PVDF) membranes (Millipore) and probed overnight at 4 °C. Primary antibody employed for the immuno-detection of kisspeptin, was anti-kisspeptin, diluted 1:200 (ab226786, Abcam). Protein levels were normalized to β-actin, as detected with anti-β-actin primary antibody, diluted 1:5000 (A5060, Sigma Aldrich); or to GAPDH, as detected with anti-GAPDH, diluted 1:500000 (ab181602, Abcam). Anti-rabbit horseradish peroxidase-conjugated secondary antibody (ab6721, Abcam) was incubated for 90-min and western blots were developed with chemiluminescence ECL Western Blotting Substrate (Thermo Scientific). Densitometric analysis of protein bands were conducted using the open-source image processing software, ImageJ (https://imagej.net/Image; Image Processing and Analysis in Java, NIH).

2.10. Serum cytokine analyses

Changes in the relative levels of circulating cytokines in were determined in plasma, using Proteome Profiler Arrays, in the different experimental groups, at the end of the treatment. Plasma from 10 to 12 animals from each group were pooled (130 μL) and loaded in the array membranes to detect levels of relevant biomarkers following the manufacturer's protocol (Proteome Profiler™ #ARY030 R&D Systems, Minneapolis, MN, USA). The average signal of the pair of duplicate spots, representing each protein, was calculated after subtraction of background values (pixel density) from negative control spots and were normalized to average values from positive control spots, using HLImage++ software (Version 22.0.0a; R&D Systems, Minneapolis, MN, USA).

2.11. RNA analyses

RNA isolation. Total RNA was isolated from hypothalamic samples, using the RNA extraction kit (Favorgen Tissue Total RNA Extraction Mini Kit, FATRK001). Manufacturer's instructions were followed in both cases. Nanodrop -10000 v.3.5.2 spectrophotometer (Nanodrop Technology®, Cambridge, UK) was used to determine RNA concentration and ratios 260/280 and 260/230.

Retro-transcription (RT) of mRNA: cDNA synthesis, free of genomic DNA (gDNA) contamination from intron-less target genes, was performed with the iScript™ gDNA Clear cDNA Synthesis Kit (BioRad Laboratories Inc., USA). When target designed primers for quantitative-PCR (qPCR) span over an intronic region (intro-containing targets), RT reaction was performed with iScript™ cDNA Synthesis kit (Bio-Rad Laboratories Inc., USA).

In both cases, 0.5 μg of RNA were used as initial RNA amount. Manufacturer's instructions were followed to prepare the reactions and two negative controls were used: RNA free sample mix for detection of genomic DNA (gDNA) contamination, and RT mix free sample for detection of external contamination. A T100™ thermal cycler (Bio-Rad, Hercules, CA, USA) was used for RT incubation. cDNA samples were 1:4 diluted and stored at −20 °C.

Retro-transcription (RT) reaction of miRNA: cDNA synthesis for miRNA quantification started from 5 ng/μL of RNA material and was performed with the miRCURY LNA RT Kit (Qiagen), following manufacturer's instructions. A T100™ thermal cycler (Bio-Rad, Hercules, CA, USA) was used for RT incubation; the cDNA obtained was stored at −20 °C.

Quantitative-PCR for mRNA: Real-time qPCR reactions were performed in duplicate using: 5 μL of diluted cDNA from previous RT, 0.5 μL of specific forward (fw) and reverse (rv) primers (10 μM), 6.25 μL of GoTaq ® qPCR master mix (Promega) and 2.75 μL of nuclease free water. A reference gene, *Rps11,* was measured together with the target gene for standardization of the RNA levels. Primer pairs were: rat Kiss1-forward: 5′-GCT GCT GCT TCT CCT CTG TG′, rat Kiss1-reverse: 5′-GCA TAC CGC GGG CCC TTT T-3′, Rps11-forward: 5′-CAT TCA GAC GGA GCG TGC TTA C-3′ and Rps11-reverse: 5′-TGC ATC TTC ATC TTC GTC AC-3′. In addition to RT negative controls, a blank control was added to the plate. A standard curve, generated from serial dilutions of a cDNA reference pool, was also included to correct the obtained Ct values and to estimate the efficiency of the primers, that was evaluated with the qPCR efficiency calculator online tool (Thermo-Fisher). qPCR reactions

were performed following GoTaq® manufacturer instructions in a CFX96™ Real-Time PCR thermocycler (Bio-Rad, Hercules, CA, USA).

Quantitative-PCR for miRNA: Immediately before reaction, cDNA samples were 1:60 diluted, and 3 μL were employed as cDNA starting material, as recommended by manufacturer. LNA™ primers rno-miR-137-3p, rno-miR-325 (Qiagen) and GoTaq ® qPCR master mix (Promega) were used, following manufacturer instructions, to perform the reaction in a CFX96™ Real-Time PCR thermocycler (Bio-Rad, Hercules, CA, USA). U6 snRNA was measured in parallel as reference, to perform relative expression normalization of our target miRNAs, by following the ΔCt method with a reference gene [37].

RT reactions and qPCR from cells. Previously to RT and qPCR reactions, RNA material obtained from lysates of cells isolated with FACS (Fluorescence Activated Cell Sorting) was inter-sample equalized considering as reference the lowest number of cells obtained per sample, in order to homogenize the starting amount of RNA material between different samples.

RT of mRNA and miRNAs from cells: 10 μL/3 μL (for mRNA/miRNA, respectively) of the inter-sample equalized cell lysate, were used as RNA starting material. Manufacturer's instructions were followed for mRNA RT reactions with the High-Capacity cDNA Reverse Transcription Kit (#4368814, Applied biosystems™, USA), where 10× random primers were included in the kit. For higher sensibility, miRNA RT reaction was performed following the TaqMan microRNA Assay (#4366596, Applied biosystems™, USA) instructions. For miRNA assay, TaqMan assay 5× specific primers are needed to perform target specific stem-loop RT and were independently purchased. Mmu-miR-137-3p (TaqMan™ MicroRNA Assay, #4427975, ID: 001129; Applied biosystems™, USA) and SNU6 RNA (TaqMan™ MicroRNA Assay, # 4427975- ID: 001973; Applied biosystems™, USA) primers were pooled in TE 1× buffer, as described by the manufacturer's instructions, prior to the performance of the RT in a T100™ thermal cycler (Bio-Rad, Hercules, CA, USA). The cDNA obtained was stored at −20 °C.

qPCR for miRNA and mRNA from cells: Quantitative PCRs were performed with 2 μL of the previously synthesized cDNA material, using the TaqMan Universal Maser mix II (Thermo Fisher, Scientific Waltham, MA). Following the manufacturer instructions, amplification was carried out in CFX96™ Real-Time PCR thermocycler (Bio-Rad, Hercules, CA). TaqMan® Gene Expression Assay primers (Applied biosystems™) employed for mRNA quantification were: Kiss1 (#4331182, ID: Mm03058560_m1) and GAPDH (#4331182 ID: Mm99999915_g1). For miRNA analysis, TaqMan® MicroRNA Assays 20× primers (Applied biosystems™) were employed: Mmu-miR-137-3p (TaqMan™ MicroRNA Assay, #4427975, ID: 001129; Applied biosystems™) and SNU6 RNA (TaqMan™ MicroRNA Assay, # 4427975- ID: 001973; Applied biosystems™). Calculation of expression levels of each target was conducted with the ΔCt method with a reference gene [37]. GAPDH and U6 snRNA served as internal reference for mRNA or miRNA analyses, respectively.

2.12. Fluorescence-Activated Cell Sorting (FACS)

FACS was performed in enzymatically dissociated hypothalamic samples from mice. First, mice were intraperitoneally anesthetized with ketamine/xylazine (2:1 ratio) and intracardially perfused with cold artificial cerebrospinal fluid solution. Brains were extracted to dissect the hypothalamus from the *Kiss1*$^{Cre:EYFP}$ mice, which were stereotaxically injected previously with viruses harboring vectors expressing miR-137-3p and mCherry under Cre activity. To perform digestion of the tissue, MBH isolation was done in cold aCSF, and was incubated for 50 min at 37 °C in aCSF-enzymatic solution containing 20 units/mL of papain (PDS Kit, LK003176, Worthington) and 0.005 % of DNase I (LK003172, Worthington). Next, tissues were mechanically dissociated by slow and soft pipetting, with progressive decreasing calibers. Then, homogenates were washed, filtered, centrifuged at 200*g* for 5 min at 4 °C, and resuspended in 500 μL of recovery solution (HBSS 1×, 5 % glucose, 0,2 % BSA, 0,02 % HCO_3^- in H_2O DEPC). Immediately, samples were placed on ice, and sorted with a FACS Aria III (Becton Dickinson) cell sorter at the Unit of Cytometry of IMIBIC. Purified cells were lysated (0.01 % Triton-X, 35 U RNasin®- Promega- in H_2O DEPC) to study RNA expression by TaqMan PCR analysis.

2.13. Immunohistochemistry

Before immunohistochemistry, brains were collected from mice intraperitoneally anesthetized with ketamine/ xylazine in a 2:1 proportion. After intracardiac blood extraction, mice were perfused with 0,9 % saline followed by 4 % of PFA. Brains were postfixed in PFA during 24 h at 4 °C, washed in PBS 24 h and dehydrated in sucrose at 30 % in PBS 0.1 M for 48 h. Brains were cut (30 μm) and divided in four sets of coronal sections in a freezing microtome (Leica CM1850 UV). One set was employed for identification of correctly infected mice, by performing immune-fluorescence against mCherry, with chicken anti-mCherry antibody (Abcam, ab205402; 1:2000); another set was used for double GFP- mCherry immunofluorescence, with chicken anti-GFP (Abcam, ab13970; 1:2000) and rabbit anti- mCherry antibody (Abcam, ab183628; 1:2000). A third set was employed for double detection of mCherry (Abcam; ab205402) and kisspeptin/NiDAB (rabbit anti rat/mouse n° 566; 1:10000; gift from A. Caraty, Nouzilly, France).

First, antigen retrieval was performed in 10 mM sodium citrate buffer, pH 6, for 10 min at 90 °C and containers were cool down under cold running tap water. Sections were blocked in 0.1 M glycine and 4 % donkey serum diluted in TBS 1×/0.3 % Triton/0.25 % BSA/ Sodium Azide 0,01 %. Sections were incubated, during 90 min at *RT* for single detection or 72 h at 4 °C for double antibody detection, with the primary antibody/antibodies diluted in incubation buffer (TBS 1×/0.3 % Triton/ 0.25 % BSA/ Sodium Azide 0,01 % and 2 % donkey serum. For single immune-fluorescence of mCherry, samples were incubated for 3 h with Alexa Fluor 555, then washed and mounted with Fluoroshield (Sigma; F6057) mounting medium. For double labelling of GPF and mCherry, GFP secondary antibody was first incubated (Biotin-SP conjugated anti-chicken), three washes were performed, and sections were incubated with Vector Elite ABC peroxidase kit (Vector Laboratories) for 90 min. Then, tree washes were done and sections were incubated 10 min with Alexa Fluor 488 Tyramide Superboost (Fisher, B40932). Next, samples were incubated for 3 h with Alexa Fluor 594 anti-rabbit, washed and mounted with Fluoroshield. For double labelling of mCherry and kisspeptin/NIDAB, Biotin-SP conjugated anti-rabbit was employed as secondary antibody anti-Kp. After ABC peroxidase step, samples were incubated with glucose oxidase and NiDAB for 20 min, washed, and incubated with Alexa Fluor 555 anti-chicken, as previously described. Finally, samples were washed, and dehydrated before mounting them with Eukitt mounting medium (ITW Reagents, 253,681).

2.14. Image acquisition and analysis

Images were taken with Leica DM2500 microscope. Kisspeptin was quantified using ImageJ. Representative sections of the arcuate nucleus were selected for each animal, including controls. For kisspeptin, images were binarized by applying the same threshold to everyone. After delimitation of the area of interest, percentage of kisspeptin signal is registered for every side of the brain section, as well as the number of mCherry expressing cells, which are visually estimated.

2.15. Bioinformatic analyses

Algorithms applied for seed-pairing prediction on *KISS1* 3'-UTR were found in these online public databases: http://www.targetscan.org/; http://www.ebi.Ac.uk/enright-srv/microcosm/htdocs/targets/v5/; http://zmf.umm.uni-heidelberg.de/apps/zmf/mirwalk2/; http://www.microrna.org/microrna/home.do. Selection of miRNA candidates was based on the criteria indicated in the Results section. As additional

miRNA-target prediction tool, we used RNA-hybrid [38], which allows prediction of multiple binding sites and the identification of the most energetically favourable hybridization sites of small RNAs (i.e., miRNAs) on large target RNAs. This is especially relevant in animal miRNAs, as these bind less tightly to target RNAs and hence more complex secondary structures of miRNA/target duplexes are formed.

2.16. Statistical analyses

Statistical analyses were performed using Prism software (GraphPad Prism version 8.0 for Windows, GraphPad Software, La Jolla, California, USA, www.graphpad.com). For each experiment, group sizes (defined as biological replicates) are shown in the figure legends. Sample sizes were set based on the previous experience of our team assessing, using rodent models, different aspects of the neuroendocrine regulation of reproductive function, and were assisted by power analyses conducted using values of standard deviation that we usually obtain when measuring parameters analogous to those studied here. Sample sizes selected were predicted to provide at least 80 % power to detect effect sizes using the tests indicated below, with a significance level of 0.05. Note, however, that according to standard procedures, in some particular cases, more complex molecular and histological analyses were implemented in a representative subset of randomly assigned samples from each group. Data represent mean ± SEM. The difference between two groups was analyzed by the unpaired Student *t*-test. Welch t-test correction was applied when SDs between groups were unequal. Differences between several groups were analyzed by one-way ANOVA (ANOVA) test followed by the Holm-Sidak test or Student-Newman-Keuls multiple comparison test. When comparing the influence of two different independent variables, experimental groups were subjected to two-way ANOVA (2-way ANOVA) followed by Student-Newman-Keuls multiple comparison test. P value of <0.05 was considered statistically significant.

For preparation of Fig. 6B, data were schematically displayed using a three-color code (white, red, green), which was applied to semi-quantitatively summarize the main effects of the obesogenic manipulations (OIH) and the different interventions (TSB, Kp-10 and T) implemented. According to this coding system: (i) white color denotes control conditions, so that any parameter that is not statistically different vs. the control group, was coded as white; (ii) red color denotes conditions that are worsened vs. controls. Any parameter that was significantly different vs. control and represented worsening of the corresponding condition, was coded as red. Of note, worsening of a given parameter may imply an increase (e.g., insulin resistance) or decrease (testosterone or LH levels) in such parameter. When a given treatment induced an intermediate situation, with significant improvement vs. the OIH condition but without full normalization, light red color was assigned (i.e., partially worsened); and (iii) green color denotes conditions that are improved vs. controls. Any parameter that was significantly different vs. control and represented an improvement in the corresponding condition, was coded as green color. Improvement of a given parameter may imply an increase or decrease in such parameter. A light green color was assigned when a treatment induced an intermediate situation (i.e., partially improved).

As standard procedure, investigators directly performing animal experimentation and analyses were not blinded to group allocation, but primary data analyses by senior authors were conducted independently to avoid any potential bias.

3. Results

3.1. The evolutionary-conserved miR-137-3p/miR-325-3p are putative regulators of Kiss1

Bioinformatic tools were applied to seek for putative miRNA regulators of the 3'-UTR of the human *KISS1* gene. The algorithms applied for seed-pairing prediction were: http://www.targetscan.org/; http://www.ebi.Ac.uk/enright-srv/microcosm/htdocs/targets/v5/; http://zmf.umm.uni-heidelberg.de/apps/zmf/mirwalk2/; and http://www.microrna.org/microrna/home.do. Selection of miRNA candidates was based on the following criteria: (i) to display evolutionary conservation at the corresponding seed region, as defined elsewhere [39], at least in mouse, rat and human; (ii) to be identified by at least one database/algorithm; and (iii) to have previous references for deregulated expression under metabolic alterations. Using these criteria, two miRNA candidate putatively capable to bind the 3'-UTR of *KISS1* were singled out: miR-137-3p and miR-325-3p. Of note, both miRNA share the same seed region for repressing *KISS1* at its 3'-UTR (Fig. S1A), which is evolutionary conserved [40], and are predicted to display relatively strong and stable interactions with *KISS1*, involving at least 8 bp (Fig. S1B). Previous unbiased analyses had evidenced that hypothalamic expression of these miRNAs is altered in conditions of metabolic stress, including high-fat content diet, in adult male rats [30]; yet, their putative role in OIH and *Kiss1* regulation had not been explored to date.

The predicted repressive interaction of miR-137-3p and miR-325-3p on *Kiss1* was experimentally tested in vitro and in vivo. First, a luciferase reporter assay was conducted using a stable cell line, HEK-293 T, transfected with a luciferase-reporter plasmid containing the 3'-UTR of the human *KISS1* gene down-stream the coding region of the chemiluminescent signal; this cell line was co-transfected with plasmids encoding the miRNA of interest. Over-expression of miR-137-3p or miR-325-3p in this cell line resulted in a significant repression of the luciferase signal (of ~20 % and 60 %, respectively), in keeping with the in silico prediction (Fig. 1A-B). In addition, the capacity of these miRNAs to repress *Kiss1* expression was assayed in vivo. To this end, and considering that both miRNAs share their seed region, adult male rats were centrally injected (intracerebroventricular; icv) with a synthetic mimetic (mimic) of miR-137-3p for 15 days. This treatment caused a marked decrease in kisspeptin (protein) content in the hypothalamus vs. the corresponding control group (Fig. 1C), together with trends for decreased LH and testosterone (T; $P = 0.059$) levels in miR-137 mimic-injected males at the end of the treatment (Fig. 1D-E).

This in vitro (human) and in vivo (rat) evidence jointly documents the conserved repressive action of the miR-137/325 tandem on *Kiss1* in a physiological setting, in line with our bioinformatic predictions. To provide further evidence supporting this interplay in the context of obesity-induced hypogonadism, hypothalamic expression analyses of miR-137-3p/miR-325-3p and *Kiss1*/kisspeptin were conducted in lean and OIH male rats. These analyses documented a consistent drop (>60 %) in *Kiss1* mRNA levels in the mediobasal hypothalamus (MBH), which encompasses the ARC, but not in the preoptic area (POA), of OIH males (Fig. 1F). Likewise, kisspeptin content in the MBH dropped >50 % in OIH males (Fig. 1G). Conversely, expression levels of miR-137-3p and miR-325-3p were significantly upregulated in OIH males, selectively in the MBH, with >130 % and 60 % rise, respectively, over control lean males (Fig. 1H-I). In contrast, no changes in expression of these miRNAs were detected in the POA of OIH males (Fig. 1H-I). However, kisspeptin content was also decreased in the POA of obese rats (Fig. 1G), suggesting additional, eventually miRNA-independent, inhibitory mechanisms at this hypothalamic site in the context of OIH, whose nature is yet to be defined.

3.2. Targeted over-expression of miR-137-3p in Kiss1 neurons partially replicates OIH in lean mice

To further document the repressive interaction between miR-137/325 and *Kiss1* in vivo, and its implication in the generation of OIH, a Cre-dependent virogenetic strategy was applied in lean male mice, to selectively over-express miR-137 in Kiss1 neurons (Fig. 2A). Using a well-validated Kiss1-Cre mouse line ($Kiss1^{Cre:GFP}$), adeno-associated viruses (AAV), harboring a vector for Cre-mediated expression of miR-137-3p and the fluorescent tag, mCherry, were bilaterally injected into

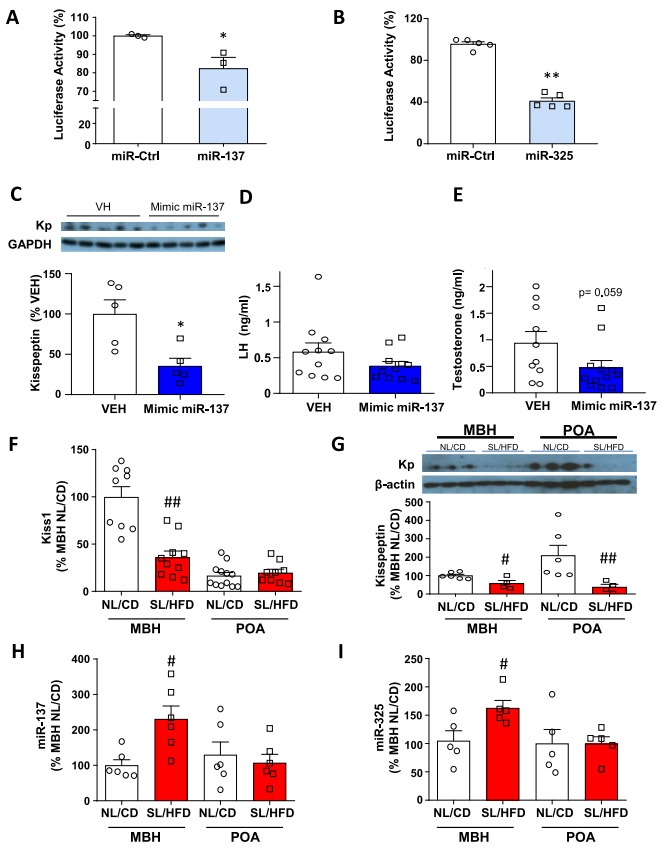

Fig. 1. miR-137-3p/miR-325-3p regulate kisspeptin expression.
(A-B) In vitro analysis of miR-137-3p/miR-325-3p regulation of *KISS1* expression. Luciferase assays were performed in cells transfected with 3'-UTR *KISS1* sequence expression plasmid and co-transfected with vectors expressing scrambled miRNA (control; miR-Ctrl) or either pre-miRNA-137-3p (A) or pre-miRNA-325-3p (B). For presentation of data, expression levels of the control miRNA group were considered 100 %, and the other values were normalized accordingly.
(C-E) Central administration of mimic-miR-137 induces downregulation of hypothalamic kisspeptin (Kp) levels as compared to control group (VEH) (C); LH and Testosterone (T) levels in mimic vs. VEH group are also shown in panels (D-E).
(F-I) Hypothalamic expression of *Kiss1* mRNA, kisspeptin protein (Kp), miR-137-3p and miR-325-3p in control (NL/CD) and OIH (SL/HFD) conditions. In (F), *Kiss1* mRNA expression levels in the MBH (including ARC) and POA of adult male rats. In (G), Kisspeptin (Kp) levels in mediobasal hypothalamus (MBH) and preoptic area (POA) of adult male rats. In (H), miR-137-3p expression in MBH and POA of adult male rats. In (I), miR-325-3p expression in MBH and POA.
For presentation of data, the level of expression of RNA or protein from MBH in control condition (NL/CD) was taken as 100 %, and the other values were normalized accordingly. Data represent mean ± SEM. Group size: $n = 3$–5 (panels A-B), $n = 6$ per group (panel C), $n = 11$ (panel D), $n = 10$–12 per group (panel E), $n = 4$–12 (panels F-I). Statistical significance was assessed by unpaired Student *t*-test. For panels F-G, comparisons were made within each hypothalamic area. $^{*}P < 0.05$, $^{**}P < 0.01$ vs miRNA control or VEH group. #P < 0.05, ##P < 0.01, ###P < 0.001 vs NL/CD (comparison within hypothalamic area: MBH or POA).

the ARC. Effective AAV delivery, infection and Cre-mediated expression of the miRNA of interest was monitored by mCherry visualization, which was detected only in Cre-positive animals, with a virtually complete colocalization of mCherry and GFP after the infection (Fig. 2B). Immunohistochemistry analysis documented a strong trend for decreased kisspeptin content in the ARC of effectively infected mice (Fig. 2C-D), with an inverse correlation between mCherry signal (denoting miR-137 expression) and kisspeptin levels. Phenotypic analyses of AAV-infected Kiss1$^{Cre:GFP}$ mice evidenced features compatible with OIH. In one hand, AVV-infected males displayed reduced LH levels at the end of the study period (Fig. 2E), in keeping with the repressive role of miR-137 on *Kiss1*/kisspeptin at the level of Kiss1 neurons. On the other hand, Cre-mediated over-expression of miR-137 in Kiss1 neurons replicated some of the metabolic complications of OIH, with elevated body weight gain and adiposity, without significant changes in energy intake (Fig. 2F-H). These metabolic changes occurred despite the limited period of follow-up (2-months) and the lack of concurrent obesogenic insults, as HFD.

In addition, qPCR analyses of Kiss1 cells in Kiss1$^{Cre:EYFP}$ control mice, isolated using EYFP signal for FACS, demonstrated that miR-137-3p is naturally expressed in the Kiss1 neuronal population (Fig. 2I-J). Moreover, qPCR analysis of Kiss1 cells infected with the AAV, isolated using EYFP and mCherry signals for FACS (Fig. 2I), showed that AVV-mediated miR-137 overexpression is bound to a significant suppression of *Kiss1* mRNA levels (Fig. 2 K-L). Altogether, these data support the validity of our approach to selectively induce miR-137-3p expression in Kiss1 neurons and repress Kiss1/kisspeptin levels.

3.3. Prevention of miR-137/325 repressive interaction on Kiss1 rescues OIH in vivo

The pathophysiological relevance of the putative miR-137/325 repression on *Kiss1* on the generation of OIH was assessed in vivo, using a validated model of obesity-induced hypogonadism in male rats, bound to metabolic and cardiovascular alterations, as well as pro-inflammatory markers. In this model, repeated central administration of Target-Site Blockers (TSB; namely TSB miR-137/325), tailored to prevent the inhibitory action of these miRNAs selectively at the *Kiss1* 3'-UTR, was applied. In our model, OIH was generated by sequential obesogenic insults, caused by overfeeding during lactation, followed by 45 % HFD after weaning up to adulthood, in line with previous references [13]. OIH male rats displayed features of (i) increased body weight and adiposity; (ii) central hypogonadism; (iii) deregulation of glucose homeostasis and insulin resistance; (iv) cardiovascular alterations; and (v) elevation of pro-inflammatory cytokines; for further details, see description of the OIH group below and Fig. 3–4.

In line with the significant suppression of hypothalamic *Kiss1* expression and kisspeptin content (see Fig. 1F-G), OIH male rats displayed also significantly reduced levels of circulating gonadotropins, LH and follicle-stimulating hormone (FSH), and testosterone (T). Repeated icv injections of TSB miR-137/325, to selectively prevent the repressive actions of miR-137/325 at the *Kiss1* 3'-UTR, to OIH male rats evoked a significant increase in hypothalamic kisspeptin levels (Fig. 3A), together with a significant elevation of LH, FSH and testosterone secretory mass, calculated as area under the curve during the treatment period (Fig. 3B-D), suggesting effective reversal of the state of central hypogonadism.

The reversal of the state of central hypogonadism in OIH males treated with TSB miR-137/325 was accompanied by a substantial improvement of the metabolic profile, despite persistent exposure to an obesogenic diet. Thus, while OIH males showed increased body weight gain and adiposity over control lean males, together with a trend for elevated leptin ($p = 0.16$) and higher basal glucose concentrations, TSB miR-137/325 administration to OIH male rats induced a significant decrease in energy intake together with a trend for reduced fat mass, despite the lack of changes in total body weight and in leptin levels (Fig. 3E-H). In addition, glucose homeostasis was significantly improved, with trends for elevation of basal insulinemia (Fig. 3I), normalization of basal glycemia (Fig. 3J), and significant attenuation of insulin resistance (Fig. 3K) and glucose intolerance (Fig. 3L) in OIH rats treated with TSB miR-137/325.

In addition, OIH males displayed signs of cardiovascular impairment, including cardiac hypertrophy and increased systolic blood pressure (SBP). Treatment of OIH males with TSB miR-137/325 reversed obesity-induced cardiac hypertrophy (Fig. 4A), and tended to reduce SBP

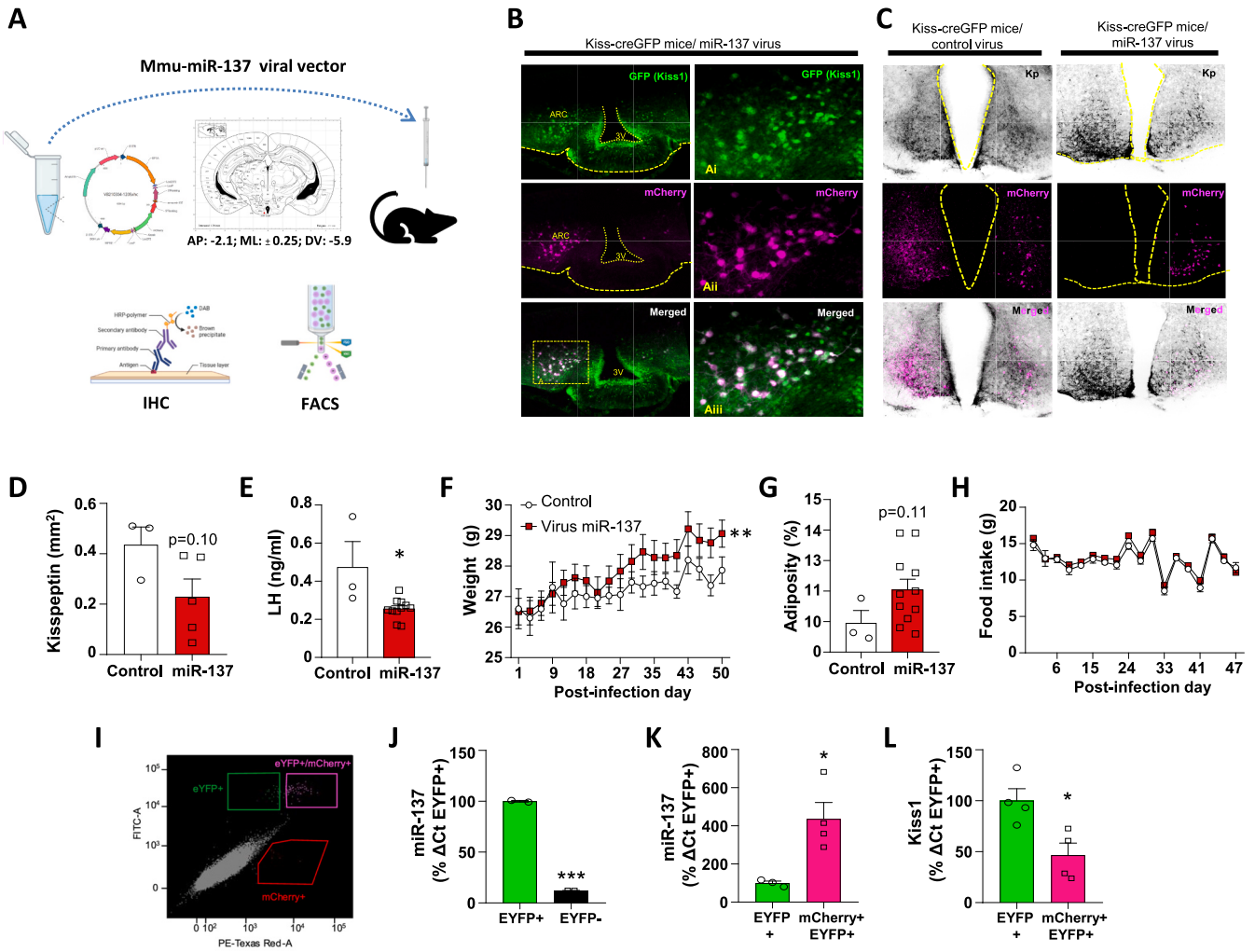

Fig. 2. Effects of Kiss1-neuron specific over-expression of miR-137 using viral vectors.

(A) Schematic representation of the strategy employed for validation of miR-137 repression in Kiss1 neurons (created with BioRender).

(B) Representative images of co-localization of GFP labelling (Kiss1-expressing cells) and infected cells with a viral construct for miR-137 over-expression (labelled by mCherry).

(C) Representative images of kisspeptin (Kp) expression reported by NiDAB, in neurons infected by the control virus, reported by mCherry (*left panels*); and NiDAB IHC and mCherry fluorescent IHC of Kiss1 neurons infected by the virus inducing miR-137 over-expression (*right panel*).

(D-E) Markers of effects of miR-137 over-expression in Kiss1 neurons, including quantification of kisspeptin IHC (defined as area with immunoreactive signal) in the ARC (D) and serum LH levels (E) in $Kiss1^{Cre:GFP}$ mice injected in the ARC with a viral vector for over-expression of miR-137 vs. control virus group.

(F-H) Metabolic markers, including evolution of body weight (F), percentage of adiposity, calculated as (fat %/fat +lean %)*100, at end of the treatment (G) and (H) Food intake in control and miR-137 over-expressing mice.

(I) FACS plot representing EYFP positive cells (FITC-A channel, in green), miR-137-mCherry positive cells (PE-Texas Red-A channel, in red) and EYFP positive cells plus miR-137-mCherry positive cells (FITC-A channel, PE-Texas Red A channel, in fuchsia).

(J) MiR-137 expression in EYFP positive cells (namely Kiss1 neurons) from control EYFP positive mice vs EYFP negative cells (i.e., non-Kiss1 cells).

(K) MiR-137 expression in EYFP positive cells (namely, Kiss1 cells not infected with the virus) against EYFP positive plus mCherry positive cells (i.e., Kiss1 cells infected with the virus for over-expression of miR-137).

(L) *Kiss1* mRNA expression analysis in double positive cells from the populations sorted by FACS.

AP: antero-posterior, ML: mediolateral, DV, dorsoventral. Data represent mean ± SEM. Group size: $n = 2–5$ in panels I-L; n = 3–11 in panels D-H. Statistical significance was assessed by 2-way ANOVA followed by Student-Newman-Keuls test (for BW and food intake) or by unpaired Student t-test. *$p < 0.05$ and **$p < 0.01$ vs control group. (For interpretation of the references to color in this figure legend, the reader is referred to the web version of this article.)

(Fig. 4B). OIH males did not display an evident difference in vascular contraction to phenylephrine (Phe), while they showed abnormal vascular relaxation responses to acetylcholine (ACh), as sign of endothelial dysfunction in mesenteric resistance arteries, which were normalized by TSB treatment (Fig. 4C-D). Further, OIH males suffered outward hypertrophic remodeling characterized by increased lumen and vessel diameters (Fig. S2A-B), wall thickness, wall:lumen ratio and vascular cross-sectional area (Fig. 4E-G), that were partially prevented by TSB administration, due to decreased wall thickness. This geometric adaptation induced by TSB treatment normalized wall stress in OIH rats (Fig. S2C). However, no differences in any parameter of vascular stiffness (i.e., strain, distensibility or stress-strain relationship) were observed between groups (Fig. S2D-F), as denoted also by lack of changes in β index (Fig. S2E, *inset*).

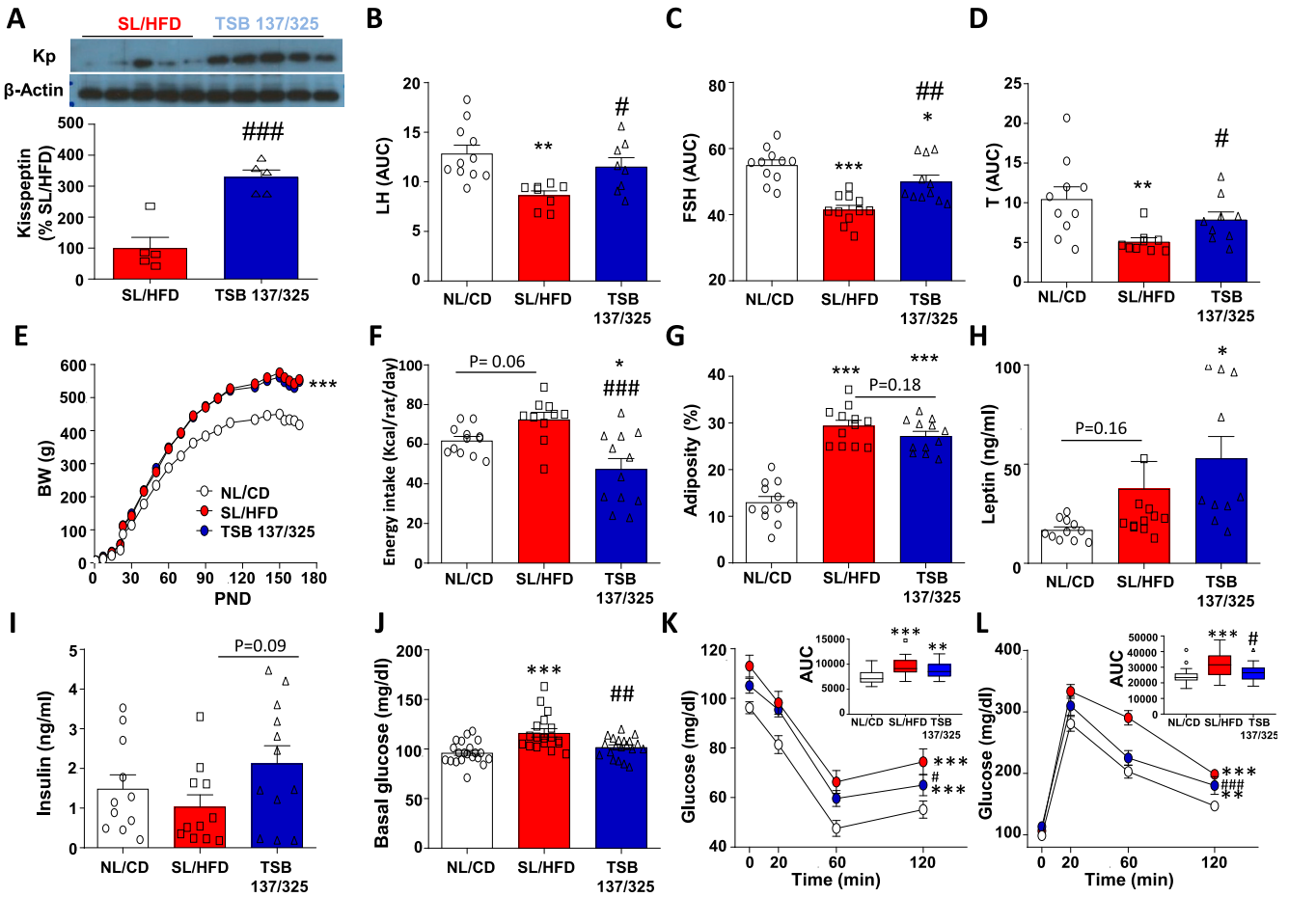

Fig. 3. Reproductive and metabolic effects of treatment with TSB miR-137/325 in a rat OIH model.
(A) Kisspeptin (Kp) protein content in the hypothalamus of OIH (SL/HFD) male rats treated with vehicle or TSB miR-137/325 (TSB 137/325).
(B-D) Reproductive indices in control lean (NL/CD) and OIH male rats, treated with either vehicle (SL/HFD) or TSB 137/325, including: integral (AUC) LH levels (B), AUC FSH levels (C), and testosterone (T) levels (D), calculated by the trapezoidal rule as area under the curve over the 15-day treatment period.
(E-J) Basic metabolic indices in control lean (NL/CD) and OIH male rats, treated with either vehicle (SL/HFD) or TSB 137/325, including: evolution of body weight (BW) from birth to the end of treatment (E), accumulated energy intake (F) and percentage of adiposity, calculated as (fat %/fat +lean%)x100, at end of the treatment (G), as well as serum leptin (H) insulin (I) and glucose (J) levels at the end of the treatment.
(K-L) Insulin and glucose tolerance tests in control lean (NL/CD) and OIH male rats, treated with either vehicle (SL/HFD) or TSB 137/325. In (K) insulin tolerance test (ITT), and in (L) glucose tolerance test (GTT) during treatment. In addition to time-course mean values, AUC (mg/dL/min) during 2 h after glucose or inulin bolus are represented (Tukey box-and-whisker plots) in the insets of panels K and L.
For presentation of protein level data, expression levels in OIH (SL/HFD) males treated with vehicle were taken as 100 %, and the other values were normalized accordingly. Data represent mean ± SEM. Group size: $n = 9$–12; except for $n = 17$–23 in panel J; $n = 20$–22 in panel K y $N = 20$–56 in panel L. Statistical significance was assessed by ANOVA followed by Holm-Sidak test or 2-way ANOVA followed by Student-Newman-Keuls test (Panels E, K and L). $^{*}P < 0.05$, $^{**}P < 0.01$, $^{***}P < 0.001$ vs control (NL/CD) and #P < 0.05, ##P < 0.01, ###P < 0.001 vs OIH condition (SL/HFD).

3.4. TSB miR-137/325 outperforms kisspeptin- or T-replacement treatments in the reversion of OIH

Given the conspicuous lack of effective therapies for OIH, and the effectiveness of our TSB strategy to reverse most of the phenotypic alterations in our OIH model, we explored whether this miRNA-based approach would outperform the efficacy of more distal pharmacological treatments, reversing the low kisspeptin tone or testosterone levels in the same OIH model. Of note, while testosterone replacement is indicated for management of severe forms of hypogonadism, pharmacological treatments based on kisspeptin administration have not been tested in obesity-induced male hypogonadism, and might actually be bound to some adverse effects, as suggested by initial studies on the impact systemic administration of high doses of kisspeptin in male rats [41].

Repeated kisspeptin-10 administration to OIH male rats was capable to enhance circulating levels of LH, FSH and T, at the end of the treatment period. Of note, final LH and T levels reached supra-physiological values as they were significantly higher than those observed in control lean males treated with vehicle (Fig. 5A-C). However, although leptin levels were normalized in kisspeptin-treated OIH males (Fig. 5F), they failed to show significant improvements of other key metabolic parameters, including body weight gain (Fig. 5D), fat mass content (Fig. 5E), or basal insulin and glucose levels (Fig. 5G-H). In addition, kisspeptin treatment did not improve insulin resistance (Fig. 5I) nor it ameliorated glucose intolerance (Fig. 5J), when compared with OIH group treated with vehicle. Regarding cardiovascular alterations, kisspeptin administration did not reverse alterations caused by OIH in terms of cardiac hypertrophy (Fig. 5K) or elevated SBP (Fig. 5L).

In turn, testosterone replacement to OIH male rats was associated with a significant decrease in serum LH and FSH levels, but massive elevation of circulating testosterone levels (Fig. 5 A-C), which were > 10- fold higher that values in the OIH group treated with vehicle; this was associated with a rise of relative prostate weight (168 ± 8 mg/100 g vs. 128 ± 8 mg/100 g BW; $P = 0.007$), when compared to the OIH group treated with vehicle. Intriguingly, while there was a trend for increased

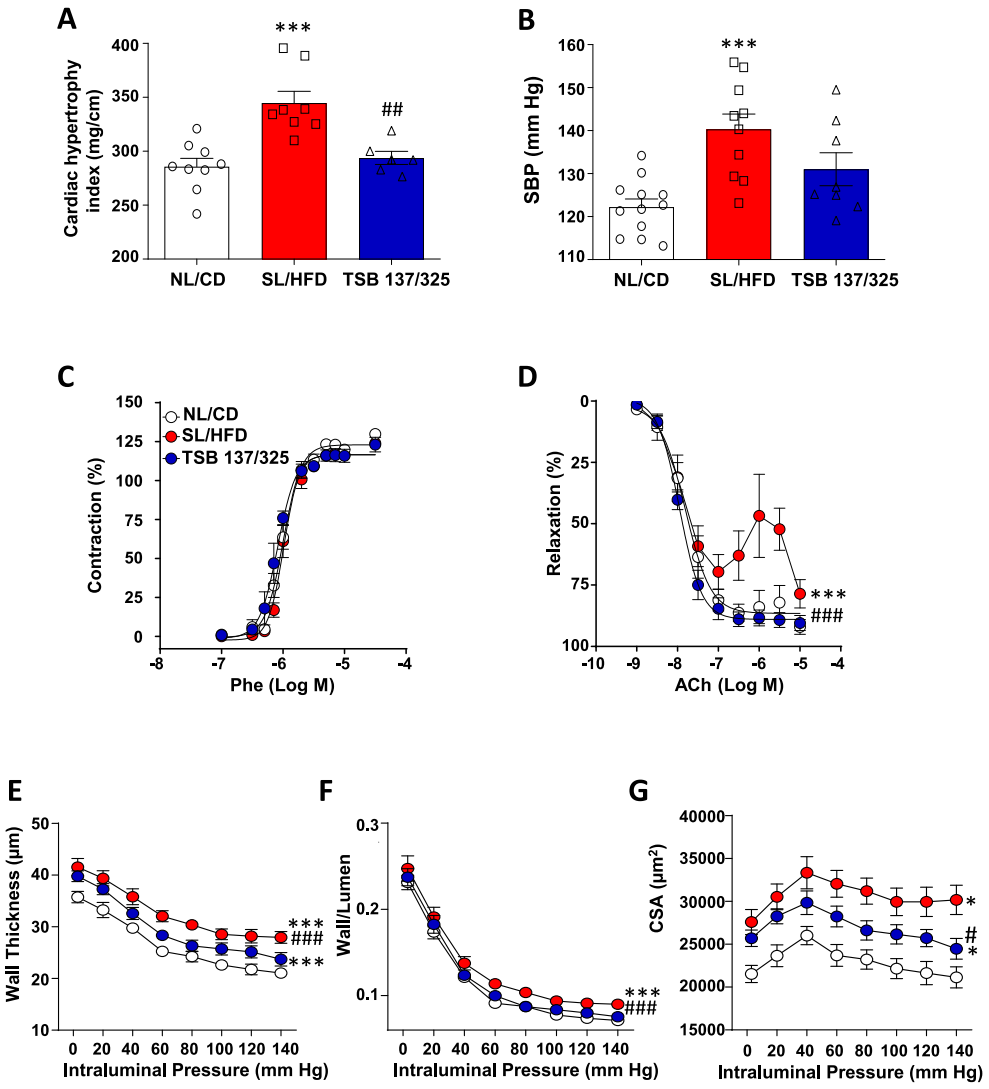

Fig. 4. Cardiovascular effects of treatment with TSB miR-137/325 in a rat OIH model.

(A) Cardiac hypertrophy in control lean (NL/CD) and OIH male rats, treated with either vehicle (SL/HFD) or TSB miR-137/325 (TSB 137/325), at the end of treatment.

(B) Systolic blood pressure (SBP), in the same groups, at the end of treatment.

(C-D) Dose-response curves of vascular contraction or relaxation in response to phenylephrine (Phe) and acetylcholine (ACh).

(E-G) Structural parameters (wall thickness, wall/lumen and CSA: cross sectional area) in mesenteric resistance arteries, of the different experimental groups; control (NL/CD); OIH (SL/HFD) treated with vehicle; or OIH (SL/HFD) treated with TSB 137/325.

Data represent mean ± SEM. Group size: $n = 5$–12. Statistical significance was assessed by 2-way ANOVA followed by Student-Newman-Keuls multiple range test. *p < 0.05, ***P < 0.001 vs control (NL/CD), and #P < 0.05, ##P < 0.01, ###P < 0.001 vs OIH condition (SL/HFD).

basal insulin levels, ITT revealed no improvement in insulin resistance caused by testosterone treatment. In addition, although basal glucose levels were reduced, GTT showed no amelioration of glucose intolerance (Fig. 5G-J). No changes were observed following testosterone administration regarding body weight, adiposity, leptin, cardiac hypertrophy or SBP (Fig. 5D-F, K-L).

Finally, while OIH males showed upregulation of serum levels of multiple pro-inflammatory cytokines, including several interleukins (IL), TNF-α, various members of the fibroblast growth factor (FGF) family and interferon (IFN), central administration of TSB miR-137/325 largely normalized the pro-inflammatory cytokine profile observed in obese male rats, including specific beneficial effects on the circulating levels of NT-4, FGF21 and IFN γ, which were not reduced in OIH males treated with either kisspeptin or testosterone. In turn, kisspeptin treatment evoked less dramatic changes in serum cytokine concentrations, with prominent amelioration of IL17A, NT-3 and prolactin levels. In addition, testosterone replacement was able to moderately improve the circulating levels of several cytokines, with marked reduction of IL1ra, IL17, CCL3, MAG and prolactin levels in OIH male rats (Fig. 6A).

A graphical summary of the main effects of the obesogenic manipulation (OIH), and the different interventions (i.e., TSB miR-137/325, Kp-10 and T) applied in this model of obesity, is presented in Fig. 6B. Note that data are semi-quantitatively displayed using a three-color code (white: within normal range; red: worsened response; green: improved response over normal values), as described in the Methods section. For further details, see the figure legend.

4. Discussion

Obesity-induced hypogonadism is a common, usually underrecognized condition that affects up to 50 % of adult men suffering long-term obesity [6,42]. Besides its potential reproductive implications, ranging from low sexual desire and erectile dysfunction to subfertility, persistently suppressed testicular function has been claimed to contribute to

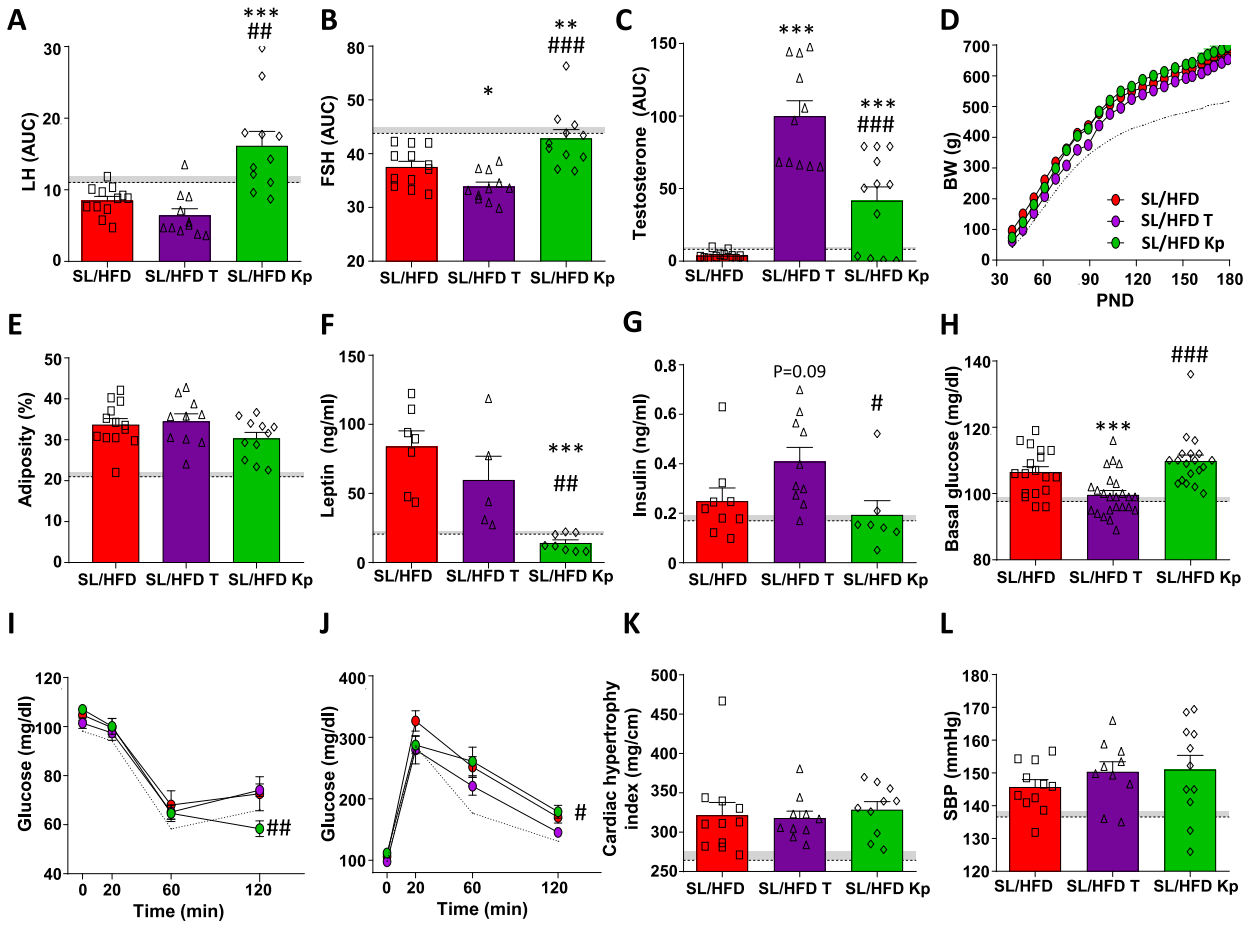

Fig. 5. Effects of treatments with either Kp-10 and testosterone (T) in the OIH model.

(A-C) Reproductive indices in OIH male rats, treated with either vehicle (SL/HFD), testosterone (T) implants or repeated injections of Kp-10; these parameters include: integral (AUC) LH levels (A), AUC FSH levels (B), and T levels (D), calculated by the trapezoidal rule as area under the curve over the 15-day treatment period.

(D-H) Basic metabolic indices in OIH male rats, treated with either vehicle (SL/HFD), T or Kp-10, including: evolution of body weight (BW) from birth to the end of treatment (D), percentage of adiposity, calculated as (fat %/fat +lean%)x100, at end of the treatment (E), and serum leptin (F) insulin (G) and basal glucose (H) levels at the end of the treatment.

(I-J) Insulin and glucose tolerance tests in OIH male rats, treated with either vehicle (SL/HFD), T or Kp-10. In (I) insulin tolerance test (ITT), and in (J) glucose tolerance test (GTT) during treatment.

(K-L) Cardiac hypertrophy and systolic blood pressure in the three groups, at the end of the treatment.

Reference values from control lean (NL/CD) male rats are displayed as dotted lines. Data represent mean ± SEM. Group size: n = 9–12; except for n = 17–23 in panel H. Statistical significance was assessed using ANOVA followed by Student-Newman-Keuls multiple range test. *P < 0.05, ***P < 0.001 vs control (SL/HFD); #P < 0.05, ##P < 0.01 and ###P < 0.001 vs SL/HFD T.

the deterioration of metabolic health, defining a sort of vicious circle, in which progressive obesity leads to greater hypogonadism, which in turn aggravates the cardiometabolic complications of overweight [43–45]. Using a male rat model of sequential exposure to obesogenic manipulations since early postnatal life, we have defined herein, by a combination of expression and functional studies, the putative pathogenic role, and eventual druggable potential, of deregulated miR-137-3p/miR-325-3p in OIH of the male, via suppression of hypothalamic kisspeptin.

MiR-137-3p is an evolutionary conserved miRNA, whose expression is highly enriched in the central nervous system in rodents and humans [46,47], including robust hypothalamic expression in rats and mice [30,48]. MiR-137 has been involved in the regulation of a wide variety of key bodily functions, ranging from the control of cell cycle to neuronal development and maturation [49]. Accordingly, perturbations in this miRNA have been associated to different conditions in humans, from oncogenesis to psychiatric disorders [49]. From a neuroendocrine perspective, miR-137 has been recently shown to target a key neuropeptide system, namely orexin/hypocretin, to regulate the wake-sleep ratio [40]; genetic variations in miR-137 locus in humans are linked to changes in sleep duration [40]. In this context, we were intrigued by our in silico analyses pointing out that miR-137-3p, and its related, miR-325-3p, which share a seed region that is totally conserved between humans and rodents, can potentially repress *Kiss1*, as pivotal element in the neuroendocrine control of the reproductive axis. Considering, in addition, that (i) unbiased analyses from our group had documented changes in the hypothalamic expression of these miRNAs in rat models of nutritional manipulation, from caloric restriction to obesity [30], and (ii) OIH in male rodent and rabbit models has been suggested to be linked, at least partially, to central suppression of *Kiss1* [12–14,50], we experimentally explored the putative function of miR-137-3p and miR-325-3p in the repressive control of hypothalamic *Kiss1* in a validated model of male OIH.

Initial functional analyses in vitro and expression data in vivo were fully compatible with this putative pathogenic role. Our reporter assays documented a significant repressive action of miR-137 and miR-325 on human *KISS1* in a heterologous cell system. Moreover, our OIH male rats not only recapitulated the main phenotypic (reproductive, hormonal and metabolic) features of obese, hypogonadal men, and displayed

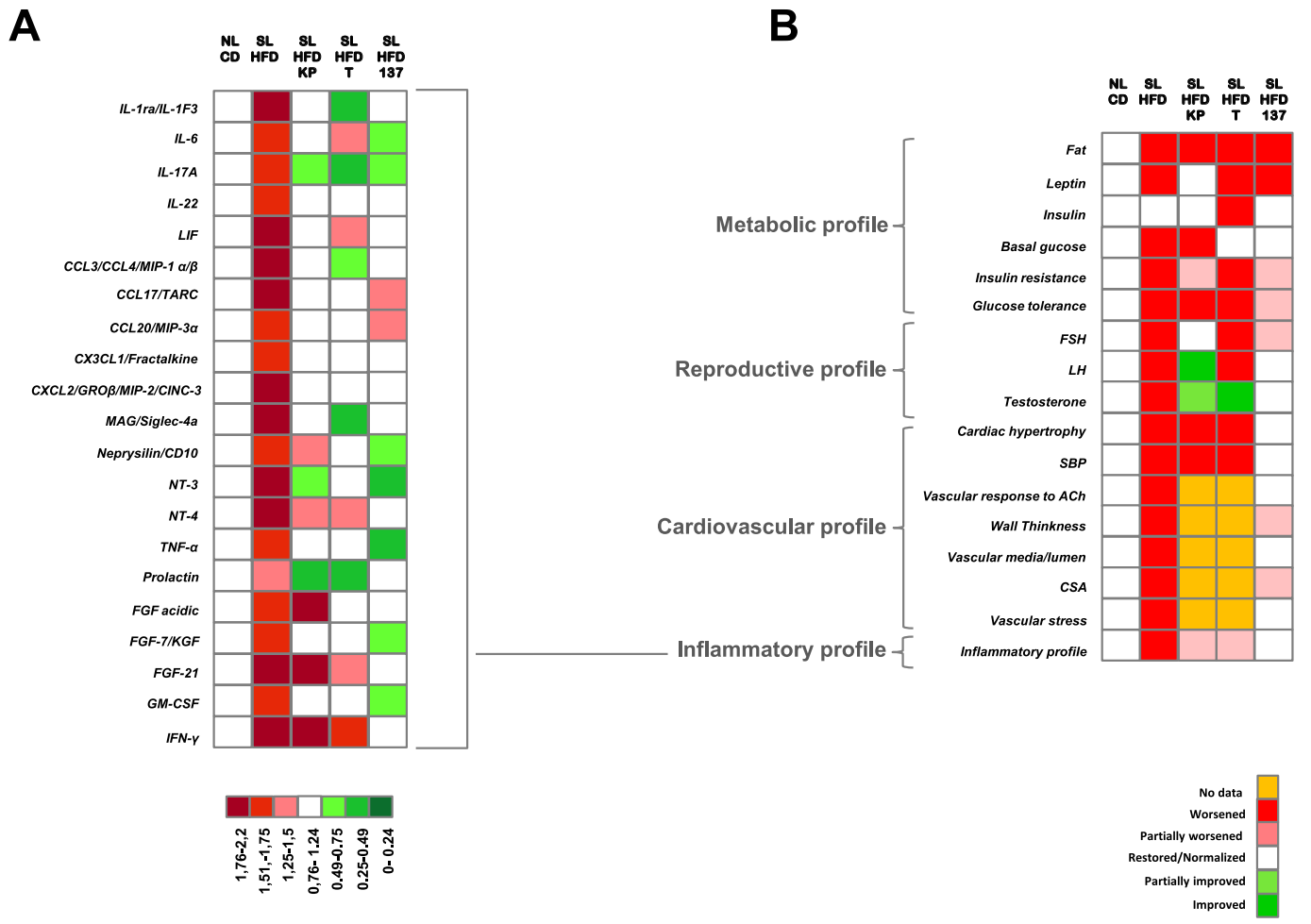

Fig. 6. Cytokine profiler and summary of cardiometabolic, reproductive and inflammatory profiles in OIH rats after different treatments.
(A) Cytokine profiles in the different experimental groups: control (NL/CD) and OIH (SL/HFD) rats, treated with vehicle, kisspeptin, testosterone, or TSB miR-137/325 (noted as 137). Data represent average density of duplicates. n = 9–12. Quantitative data are presented as heatmap, following the color-codes included in the panel.
(B) Graphical summary in the form of semi-quantitative heatmap of changes in the multiple parameters evaluated in OIH (vs. control NL/CD represented in white) and the effect of the different treatments: kisspeptin (Kp-10), testosterone (T) or TSB miR-137/325 in OIH males. Quantitative data are presented in Figs. 2 to 6A. Semi-quantitative representation of the data was done using a three color-code, included in the panel and described in the Methods section. Parameters in white are within the range of normality, while parameters in red are significantly worsened by the obesogenic manipulation and/or the pharmacological intervention(s). Parameters in green represent improved responses vs. control reference values. Squares in orange represent data not available. (For interpretation of the references to color in this figure legend, the reader is referred to the web version of this article.)

decreased hypothalamic expression of *Kiss1* and kisspeptin content, mainly in the MBH, where the prominent population of ARC Kiss1 neurons is located [15], but showed also increased levels of miR-137-3p and miR-325-3p in this hypothalamic area. Such inverse relationship between the hypothalamic (MBH) levels of expression of *Kiss1*/kisspeptin (decreased) and miR-137-3p/miR-325-3p (increased) is congruent with a putative repressive role of these miRNAs on *Kiss1*/kisspeptin expression in the context of OIH. The findings from our in vivo experiments in lean adult males, in which central administration of a synthetic mimic of miR-137-3p caused a significant suppression of kisspeptin content, together with a strong trend for decreased T and LH levels, further support a mechanistic role of elevated miR-137-3p and miR-325-3p levels as driving force for the suppression of kisspeptin in the mediobasal hypothalamus and, thereby, the reproductive axis in obese male rats.

More incisive approaches, involving miRNA expression analyses and selective over-expression of miR-137-3p in Kiss1 neurons in vivo, further confirmed this putative miRNA/*Kiss1* repressive pathway in male rodents. Note that due to their technical complexity and the fact that miR-137-3p and miR-325-3p share their seed region, these analyses were only conducted for the former miRNA. Using an engineered mouse line to selectively express Cre recombinase and suitable fluorescent markers specifically in Kiss1 cells, we are the first to demonstrate that miR-137-3p is actually expressed by Kiss1 neurons from the MBH, isolated using FACS. Additionally, by employing ARC stereotaxic delivery of viral vectors in this mouse line in order to induce miR-137 over-expression in a Cre-dependent manner, our study conclusively documents a repressive action of miR-137 on *Kiss1* in vivo, as elevated miR-137 levels in Kiss1 neurons were associated to a drop in *Kiss1* expression, together with a suppression of markers of reproductive axis function, such as circulating LH levels, in lean male mice. Interestingly, over-expression of miR-137 in Kiss1 cells caused also an elevation of body weight and tended to increase adiposity, in absence of any obesogenic diet, further supporting the contribution of enhanced miR-137 expression in this neuronal population to the metabolic phenotype of diet-induced obese males.

Based on these expression and functional data, we assessed also whether preventing the repressive interplay between endogenous miR-137-3p/miR-325-3p and *Kiss1* in vivo may ameliorate the reproductive and metabolic traits of OIH observed in our rat model, using a TSB strategy. Of important note, due to its specific design, our TSB miR-137/

325 permits selective blockade of the repressive interaction of both miR-137 and miR-325 selectively at their specific binding site in the 3'-UTR of *Kiss1*. Our data conclusively demonstrate that by specifically interfering the repressive action of this miRNA tandem on the 3'-UTR of *Kiss1*, the state of OIH can be largely reversed, with a detectable increase in integral LH, FSH and T levels, together with a substantial elevation in the hypothalamic content of kisspeptin, despite persistent exposure to the obesogenic diet. Interestingly, the effects of this TSB on reproductive hormone parameters and hypothalamic kisspeptin content were bound to a significant suppression of daily energy intake, which is congruent with the previously reported anorexigenic effect of kisspeptin [51,52], together with a marked improvement of key metabolic indices in OIH males, including partial correction of glucose intolerance, insulin resistance and cardiac hypertrophy (as index of increased peripheral vascular resistance), as well as trends for reversion of excess of adiposity and elevated systolic blood pressure. In addition, different indices of vascular reactivity and the pro-inflammatory cytokine profile of obese male rats suffering central hypogonadism were largely improved or even normalized by the TSB treatment. Given the central and specific targeting of *Kiss1* with our TSB approach, the most tenable mechanistic explanation for the amelioration of the metabolic and cardiovascular phenotypes in OIH males is the primary reversal of central hypogonadism in our model. Overall, our findings not only support a major pathogenic role of deregulated miR-137-3p and miR-325-3p expression at the hypothalamus for the generation of the constellation of alterations of OIH, but also pave the way for the potential use of TSB-based therapies for effective management of obesity and hypogonadism of the male.

Not only central hypogonadism associated to obesity is usually under-diagnosed, but the therapeutic options to properly manage this condition are either symptomatic (i.e., do not target the basis of the disease) or of limited efficacy. The initial mainstay for handling low testosterone levels in obese men consists of lifestyle changes, since modification of alimentary habits and promotion of physical exercise can improve also gonadal function [5,53]. Yet, this first-line intervention is often unsuccessful and additional treatments, ranging from bariatric surgery to GLP-1 analogues or testosterone replacement have been employed. Testosterone supplementation might allow correction of hypogonadism, and therefore, may reverse the pathogenic basis of some of manifestations of OIH. In this context, different formulations of testosterone have been advocated in the pharmacological treatment of OIH, to increase circulating androgen levels and reduce insulin resistance [54]. However, testosterone treatments are not exempted from potentially adverse side-effects [5,53], so that their risk/benefit ratio remains strongly controversial, with lack of robust data on its long-term clinical efficacy [55,56]. In addition, given the evidence for decreased kisspeptin tone in models of OIH in rodents and rabbits, replacement therapies to correct central hypogonadism in obese men involving kisspeptin administration might be also considered, especially since pilot clinical evidence strongly suggested the efficacy of kisspeptin-10 administration to enhance testosterone and LH levels in men suffering type-2 diabetes and mild hypogonadism [57].

In this context, we found relevant to compare the efficacy of our protocol of central TSB administration with that of treatment with T implants or repeated kisspeptin-10 administration, as alternative means to rescue hypogonadism in our model. Our comparative data clearly documented that repeated TSB administration outperforms the efficacy of pharmacological treatments with either kisspeptin-10 or T in terms of integral reversion of the metabolic and inflammatory traits of OIH in our rat model (see Fig. 6B). Importantly, of the three protocols tested, only the TSB miR-137/325 allowed a partial reversion of the central hypogonadal state without causing supra-physiological levels of gonadotropins and/or testosterone. Hence, it can be argued that, while restoration of the physiological levels of *Kiss1* expression and circulating gonadotropins/testosterone, by preventing the repressive action of miR-137-3p and miR-325-3p at the hypothalamus, is optimal to reverse most of the cardinal manifestations of OIH, the pharmacological effects of either kisspeptin-10 or T replacement, while improving some parameters, are clearly inappropriate to globally ameliorate the metabolic and inflammatory profile of obese male rats, as they cause also supraphysiological stimulation of gonadotropin or testosterone levels. While improved outcomes might be achieved by changes in dosage and temporal protocols of administration of kisspeptins or T, our present findings may have important translational implications for future design of personalized strategies for the pharmacological management of OIH in men, in which targeted vectors, as nanoparticles or small extracellular vesicles (sEV), might be used to cargo and deliver LNA-based TSB into the central nervous system for effective transduction of Kiss1 neurons in vivo, in line with recent evidence suggesting effective brain targeting of systemically administered nucleotide vectors in sEV carriers [58]. This reinforces the translational dimension of our data, that help for a better understanding of the underlying basis and improved management of a highly prevalent, but frequently overlooked condition among men suffering obesity.

Supplementary data to this article can be found online at https://doi.org/10.1016/j.metabol.2024.155932.

Funding

This work was supported by the following grants:

- BFU2017-83934-P and PID2020-118660 GB-I00 (to MTS; Agencia Estatal de Investigación, Spain; co-funded with EU funds from FEDER Program);
- PI21/01770 (to MSA; Instituto de Salud Carlos III, Spain);
- Projects PIE14-00005 and DTS20/00117 (to MTS; Instituto de Salud Carlos III);
- Projects P12-FQM-01943 and P18-RT-4093 (to MTS) and PI-0323-20 (to MSA; Junta de Andalucía, Spain);
- Project 1254821 (to MTS, University of Cordoba-FEDER);
- Miguel Servet Program (to MSA, CP 19/00195, Instituto de Salud Carlos III);
- EU research contracts GAP-2014-655232 and GAP-101080219 (eprObes; funded by the European Union through the Horizon Europe Framework Programme);
- CIBER is an initiative of Instituto de Salud Carlos III (Ministerio de Sanidad, Spain).

CRediT authorship contribution statement

María S. Avendaño: Writing – review & editing, Writing – original draft, Validation, Supervision, Methodology, Investigation, Funding acquisition, Formal analysis, Data curation, Conceptualization. **Cecilia Perdices-Lopez:** Writing – review & editing, Writing – original draft, Visualization, Validation, Methodology, Investigation, Formal analysis, Data curation. **Yolanda Guerrero-Ruiz:** Writing – review & editing, Methodology, Investigation. **Francisco Ruiz-Pino:** Writing – review & editing, Methodology, Investigation. **Ana B. Rodriguez-Sanchez:** Methodology, Investigation. **María J. Sanchez-Tapia:** Methodology, Investigation. **Verónica Sobrino:** Writing – review & editing, Methodology, Investigation. **Rafael Pineda:** Writing – review & editing, Methodology, Investigation. **Alexia Barroso:** Writing – review & editing, Methodology, Investigation. **Alejandro Correa-Sáez:** Writing – review & editing, Methodology, Investigation. **Maribel Lara-Chica:** Writing – review & editing, Methodology, Investigation. **José C. Fernandez-Garcia:** Writing – review & editing, Investigation, Formal analysis. **Ana B. García-Redondo:** Writing – review & editing, Methodology, Investigation, Formal analysis. **Raquel Hernanz:** Writing – review & editing, Methodology, Investigation, Formal analysis. **Miguel Ruiz-Cruz:** Writing – review & editing, Methodology, Investigation. **David Garcia-Galiano:** Writing – review & editing, Methodology, Investigation, Formal analysis. **Nelly Pitteloud:** Writing – review &

editing, Validation, Formal analysis, Conceptualization. **Marco A. Calzado:** Writing – review & editing, Validation, Investigation, Formal analysis. **Ana M. Briones:** Writing – review & editing, Writing – original draft, Validation, Methodology, Investigation, Formal analysis. **María J. Vázquez:** Writing – review & editing, Supervision, Methodology, Investigation, Formal analysis, Conceptualization. **Manuel Tena-Sempere:** Writing – review & editing, Writing – original draft, Validation, Supervision, Project administration, Methodology, Funding acquisition, Conceptualization.

Declaration of competing interest

The authors have no conflict of interest to disclose in relation to the contents of this work.

Data availability

The authors confirm that all data are available in the main text or the supplementary materials. Contents in the Methods, Results and Discussion sections of this article are part of the Doctoral Thesis of Cecilia Perdices-Lopez, that per academic normative has been deposited in the institutional electronic repository of the University of Cordoba, https://helvia.uco.es.

References

[1] Chooi YC, Ding C, Magkos F. The epidemiology of obesity. Metabolism 2019;92:6–10.
[2] Bluher M. Obesity: global epidemiology and pathogenesis. Nat Rev Endocrinol 2019;15:288–98.
[3] Drucker DJ. Diabetes, obesity, metabolism, and SARS-CoV-2 infection: the end of the beginning. Cell Metab 2021;33:479–98.
[4] Tajar A, Forti G, O'Neill TW, Lee DM, Silman AJ, Finn JD, et al. Characteristics of secondary, primary, and compensated hypogonadism in aging men: evidence from the European Male Ageing Study. J Clin Endocrinol Metab 2010;95:1810–8.
[5] Molina-Vega M, Munoz-Garach A, Damas-Fuentes M, Fernandez-Garcia JC, Tinahones FJ. Secondary male hypogonadism: a prevalent but overlooked comorbidity of obesity. Asian J Androl 2018;20:531–8.
[6] Calderon B, Gomez-Martin JM, Vega-Pinero B, Martin-Hidalgo A, Galindo J, Luque-Ramirez M, et al. Prevalence of male secondary hypogonadism in moderate to severe obesity and its relationship with insulin resistance and excess body weight. Andrology 2016;4:62–7.
[7] Erenpreiss J, Fodina V, Pozarska R, Zubkova K, Dudorova A, Pozarskis A. Prevalence of testosterone deficiency among aging men with and without morbidities. Aging Male 2020;23:901–5.
[8] Heydari H, Ghiasi R, Ghaderpour S, Keyhanmanesh R. The mechanisms involved in obesity-induced male infertility. Curr Diabetes Rev 2021;17:259–67.
[9] Genchi VA, Rossi E, Lauriola C, D'Oria R, Palma G, Borrelli A, et al. Adipose tissue dysfunction and obesity-related male hypogonadism. Int J Mol Sci 2022;23:8194.
[10] Peppa M, Manta A. Sexual dysfunction in diabetic patients: Tauhe role of advanced glycation end products. Curr Diabetes Rev 2024;20:e070423215531.
[11] AbbasiHormozi S, Kouhkan A, Shahverdi A, Parikar A, Shirin A, Vesali S. How much obesity and diabetes do impair male fertility? Reprod Biol Endocrinol 2023;21:48.
[12] Quennell JH, Howell CS, Roa J, Augustine RA, Grattan DR, Anderson GM. Leptin deficiency and diet-induced obesity reduce hypothalamic kisspeptin expression in mice. Endocrinology 2011;152:1541–50.
[13] Sanchez-Garrido MA, Ruiz-Pino F, Manfredi-Lozano M, Leon S, Garcia-Galiano D, Castano JP, et al. Obesity-induced hypogonadism in the male: premature reproductive neuroendocrine senescence and contribution of Kiss1-mediated mechanisms. Endocrinology 2014;155:1067–79.
[14] Minabe S, Iwata K, Tsuchida H, Tsukamura H, Ozawa H. Effect of diet-induced obesity on kisspeptin-neurokinin B-dynorphin A neurons in the arcuate nucleus and luteinizing hormone secretion in sex hormone-primed male and female rats. Peptides 2021;142:170546.
[15] Sobrino V, Avendano MS, Perdices-Lopez C, Jimenez-Puyer M, Tena-Sempere M. Kisspeptins and the neuroendocrine control of reproduction: recent progress and new frontiers in kisspeptin research. Front Neuroendocrinol 2022;65:100977.
[16] Seminara SB, Messager S, Chatzidaki EE, Thresher RR, Acierno Jr JS, Shagoury JK, et al. The GPR54 gene as a regulator of puberty. N Engl J Med 2003;349:1614–27.
[17] d'Anglemont de Tassigny X, Fagg LA, Dixon JP, Day K, Leitch HG, Hendrick AG, et al. Hypogonadotropic hypogonadism in mice lacking a functional Kiss1 gene. Proc Natl Acad Sci USA 2007;104:10714–9.
[18] Topaloglu AK, Tello JA, Kotan LD, Ozbek MN, Yilmaz MB, Erdogan S, et al. Inactivating KISS1 mutation and hypogonadotropic hypogonadism. N Engl J Med 2012;366:629–35.
[19] Castellano JM, Navarro VM, Fernandez-Fernandez R, Nogueiras R, Tovar S, Roa J, et al. Changes in hypothalamic KiSS-1 system and restoration of pubertal activation of the reproductive axis by kisspeptin in undernutrition. Endocrinology 2005;146:3917–25.
[20] Castellano JM, Navarro VM, Fernandez-Fernandez R, Roa J, Vigo E, Pineda R, et al. Expression of hypothalamic KiSS-1 system and rescue of defective gonadotropic responses by kisspeptin in streptozotocin-induced diabetic male rats. Diabetes 2006;55:2602–10.
[21] Castellano JM, Bentsen AH, Romero M, Pineda R, Ruiz-Pino F, Garcia-Galiano D, et al. Acute inflammation reduces kisspeptin immunoreactivity at the arcuate nucleus and decreases responsiveness to kisspeptin independently of its anorectic effects. Am J Physiol Endocrinol Metab 2010;299:E54–61.
[22] Han SY, Morris PG, Kim JC, Guru S, Pardo-Navarro M, Yeo SH, et al. Mechanism of kisspeptin neuron synchronization for pulsatile hormone secretion in male mice. Cell Rep 2023;42:111914.
[23] Toro CA, Aylwin CF, Lomniczi A. Hypothalamic epigenetics driving female puberty. J Neuroendocrinol 2018;30:e12589.
[24] Tafrihi M, Hasheminasab E. MiRNAs: biology, biogenesis, their web-based tools, and databases. Microrna 2019;8:4–27.
[25] Bartel DP. Metazoan microRNAs. Cell 2018;173:20–51.
[26] Mendes ND, Freitas AT, Sagot MF. Current tools for the identification of miRNA genes and their targets. Nucleic Acids Res 2009;37:2419–33.
[27] Redis RS, Calin S, Yang Y, You MJ, Calin GA. Cell-to-cell miRNA transfer: from body homeostasis to therapy. Pharmacol Ther 2012;136:169–74.
[28] Messina A, Langlet F, Chachlaki K, Roa J, Rasika S, Jouy N, et al. A microRNA switch regulates the rise in hypothalamic GnRH production before puberty. Nat Neurosci 2016;19:835–44.
[29] Roa J, Ruiz-Cruz M, Ruiz-Pino F, Onieva R, Vazquez MJ, Sanchez-Tapia MJ, et al. Dicer ablation in Kiss1 neurons impairs puberty and fertility preferentially in female mice. Nat Commun 2022;13:4663.
[30] Sangiao-Alvarellos S, Pena-Bello L, Manfredi-Lozano M, Tena-Sempere M, Cordido F. Perturbation of hypothalamic microRNA expression patterns in male rats after metabolic distress: impact of obesity and conditions of negative energy balance. Endocrinology 2014;155:1838–50.
[31] Romero-Ruiz A, Avendano MS, Dominguez F, Lozoya T, Molina-Abril H, Sangiao-Alvarellos S, et al. Deregulation of miR-324/KISS1/kisspeptin in early ectopic pregnancy: mechanistic findings with clinical and diagnostic implications. Am J Obstet Gynecol 2019;220(480):e1–17.
[32] Padilla SL, Johnson CW, Barker FD, Patterson MA, Palmiter RD. A neural circuit underlying the generation of hot flushes. Cell Rep 2018;24:271–7.
[33] Srinivas S, Watanabe T, Lin CS, William CM, Tanabe Y, Jessell TM, et al. Cre reporter strains produced by targeted insertion of EYFP and ECFP into the ROSA26 locus. BMC Dev Biol 2001;1:4.
[34] Navarro VM, Castellano JM, Fernandez-Fernandez R, Tovar S, Roa J, Mayen A, et al. Characterization of the potent luteinizing hormone-releasing activity of KiSS-1 peptide, the natural ligand of GPR54. Endocrinology 2005;146:156–63.
[35] Avendano MS, Garcia-Redondo AB, Zalba G, Gonzalez-Amor M, Aguado A, Martinez-Revelles S, et al. mPGES-1 (microsomal prostaglandin E synthase-1) mediates vascular dysfunction in hypertension through oxidative stress. Hypertension 2018;72:492–502.
[36] Avendano MS, Martinez-Revelles S, Aguado A, Simoes MR, Gonzalez-Amor M, Palacios R, et al. Role of COX-2-derived PGE2 on vascular stiffness and function in hypertension. Br J Pharmacol 2016;173:1541–55.
[37] Pfaffl MW. A new mathematical model for relative quantification in real-time RT-PCR. Nucleic Acids Res 2001;29:e45.
[38] Rehmsmeier M, Steffen P, Hochsmann M, Giegerich R. Fast and effective prediction of microRNA/target duplexes. RNA 2004;10:1507–17.
[39] Lewis BP, Burge CB, Bartel DP. Conserved seed pairing, often flanked by adenosines, indicates that thousands of human genes are microRNA targets. Cell 2005;120:15–20.
[40] Holm A, Possovre ML, Bandarabadi M, Moseholm KF, Justinussen JL, Bozic I, et al. The evolutionarily conserved miRNA-137 targets the neuropeptide hypocretin/orexin and modulates the wake to sleep ratio. Proc Natl Acad Sci USA 2022;119:e2112225119.
[41] Thompson EL, Amber V, Stamp GW, Patterson M, Curtis AE, Cooke JH, et al. Kisspeptin-54 at high doses acutely induces testicular degeneration in adult male rats via central mechanisms. Br J Pharmacol 2009;156:609–25.
[42] Dandona P, Dhindsa S. Update: hypogonadotropic hypogonadism in type 2 diabetes and obesity. J Clin Endocrinol Metab 2011;96:2643–51.
[43] Peterson MD, Belakovskiy A, McGrath R, Yarrow JF. Testosterone deficiency, weakness, and multimorbidity in men. Sci Rep 2018;8:5897.
[44] Dandona P, Dhindsa S, Ghanim H, Saad F. Mechanisms underlying the metabolic actions of testosterone in humans: a narrative review. Diabetes Obes Metab 2021;23:18–28.
[45] Molina-Vega M, Asenjo-Plaza M, Garcia-Ruiz MC, Varea-Marineto E, Casal-Nievas N, Alvarez-Millan JJ, et al. Cross-sectional, primary care-based study of the prevalence of hypoandrogenemia in nondiabetic young men with obesity. Obesity (Silver Spring) 2019;27:1584–90.
[46] Lagos-Quintana M, Rauhut R, Yalcin A, Meyer J, Lendeckel W, Tuschl T. Identification of tissue-specific microRNAs from mouse. Curr Biol 2002;12:735–9.
[47] Landgraf P, Rusu M, Sheridan R, Sewer A, Iovino N, Aravin A, et al. A mammalian microRNA expression atlas based on small RNA library sequencing. Cell 2007;129:1401–14.
[48] Herzer S, Silahtaroglu A, Meister B. Locked nucleic acid-based in situ hybridisation reveals miR-7a as a hypothalamus-enriched microRNA with a distinct expression pattern. J Neuroendocrinol 2012;24:1492–504.
[49] Mahmoudi E, Cairns MJ. MiR-137: an important player in neural development and neoplastic transformation. Mol Psychiatry 2017;22:44–55.

[50] Morelli A, Filippi S, Comeglio P, Sarchielli E, Cellai I, Pallecchi M, et al. Physical activity counteracts metabolic syndrome-induced hypogonadotropic hypogonadism and erectile dysfunction in the rabbit. Am J Physiol Endocrinol Metab 2019;316. E519-E35.
[51] Cazarez-Marquez F, Eliveld J, Ritsema W, Foppen E, Bossenbroek Y, Pelizzari S, et al. Role of central kisspeptin and RFRP-3 in energy metabolism in the male Wistar rat. J Neuroendocrinol 2021;33:e12973.
[52] Dong TS, Vu JP, Oh S, Sanford D, Pisegna JR, Germano P. Intraperitoneal treatment of kisspeptin suppresses appetite and energy expenditure and alters gastrointestinal hormones in mice. Dig Dis Sci 2020;65:2254–63.
[53] Fernandez CJ, Chacko EC, Pappachan JM. Male obesity-related secondary hypogonadism - pathophysiology, clinical implications and management. Eur Endocrinol 2019;15:83–90.
[54] Dhindsa S, Miller MG, McWhirter CL, Mager DE, Ghanim H, Chaudhuri A, et al. Testosterone concentrations in diabetic and nondiabetic obese men. Diabetes Care 2010;33:1186–92.
[55] Nguyen CP, Hirsch MS, Moeny D, Kaul S, Mohamoud M, Joffe HV. Testosterone and "age-related hypogonadism"–FDA concerns. N Engl J Med 2015;373:689–91.
[56] Grossmann M. Hypogonadism and male obesity: focus on unresolved questions. Clin Endocrinol 2018;89:11–21.
[57] George JT, Veldhuis JD, Tena-Sempere M, Millar RP, Anderson RA. Exploring the pathophysiology of hypogonadism in men with type 2 diabetes: kisspeptin-10 stimulates serum testosterone and LH secretion in men with type 2 diabetes and mild biochemical hypogonadism. Clin Endocrinol 2013;79:100–4.
[58] Milbank E, Dragano NRV, Gonzalez-Garcia I, Garcia MR, Rivas-Limeres V, Perdomo L, et al. Small extracellular vesicle-mediated targeting of hypothalamic AMPKalpha1 corrects obesity through BAT activation. Nat Metab 2021;3:1415–31.